J. Fluid Mech. (2010), *vol.* 664, *pp.* 478–509.
doi:10.1017/S0022112010003812

Inertia-gravity waves beyond the inertial latitude. Part 1. Inviscid singular focusing

VICTOR I. SHRIRA† AND WILLIAM A. TOWNSEND

Department of Mathematics, EPSAM, Keele University, Keele ST5 5BG, UK

(Received 17 December 2009; revised 12 July 2010; accepted 12 July 2010;
first published online 15 October 2010)

The paper is concerned with analytical study of inertia-gravity waves in rotating density-stratified ideal fluid confined in a spherical shell. It primarily aims at clarifying the possible role of these motions in deep ocean mixing. Recently, it was found that on the 'non-traditional' β-plane inertia-gravity internal waves can propagate polewards beyond their inertial latitude, where the wave frequency equals the local Coriolis parameter, by turning into subinertial modes trapped in the narrowing waveguides around the local minima of buoyancy frequency N. The behaviour of characteristics was established: wave horizontal and vertical scales decrease as the wave advances polewards and tend to zero at a latitude corresponding to an attractor of characteristics. However, the basic questions about wave evolution, its quantitative description and the possibility of its reflection from the critical latitude remain open. The present work addresses these issues by studying the linear inviscid evolution of finite bandwidth wavepackets on the 'non-traditional' β-plane past the inertial latitude for generic oceanic stratification. Beyond the inertial latitude, the wave field is confined in narrowing waveguides of three distinct generic types around different local minima of the buoyancy frequency. In the oceanic context, the widest is adjacent to the flat bottom, the thinnest is the upper mixed layer, and the middle one is located between the seasonal and main thermocline. We find explicit asymptotic solutions describing the wave field in the WKB approximation. As a byproduct, the conservation of wave action principle is explicitly formulated for all types of internal waves on the 'non-traditional' β-plane. The wave velocities and vertical shear tend to infinity and become singular at the attractor latitude or its vicinity for both monochromatic and finite bandwidth packets. We call this phenomenon *singular focusing*. These WKB solutions are shown to remain valid up to singularity for the bottom and mid-ocean waveguides. The main conclusion is that even in the inviscid setting the wave evolution towards smaller and smaller horizontal and vertical scales is irreversible: there is no reflection. For situations typical of deep ocean, a simultaneous increase in wave amplitude and decrease of vertical scale causes a sharp increase of vertical shear, which may lead to wave breaking and increased mixing.

Key words: internal waves, rotating flows, waves in rotating fluids

1. Introduction

The primary motivation for this work comes from physical oceanography. In the ocean, internal waves of inertial band are by far the most energetic, and whatever

† Email address for correspondence: v.i.shrira@keele.ac.uk

happens to this band affects internal waves of all scales (e.g. Fu 1981; Garrett 2001). Inertial waves enhance vertical mixing (e.g. Alford 2003) and, in particular, are believed to play a major role in deep ocean mixing (Wunsch & Munk 1998; Garrett & St Laurent 2002). Although general mechanisms of mixing are well established (e.g. Staquet 2004), it is not clear how waves evolve to breaking conditions. The key question is whether the mechanism is the cascade of weakly nonlinear resonant wave interactions, which does provide energy transfer to small vertical scales and hence to strong vertical shear (e.g. Winters & D'Asaro 1997), or if there are alternatives. In this paper, we argue that a plausible alternative does exist and could be provided by a linear transformation of inertia-gravity waves into small vertical and horizontal scales which was found to occur on the non-traditional β-plane (Gerkema & Shrira 2005*a*, *b*).

Similar open questions about the role of inertia-gravity waves in mixing are not confined to oceanic context, but are also relevant to transport processes in stars (e.g. Kumar & Quataert 1997; Zahn 1997), atmospheres and liquid core of the Earth (Rieutord *et al.* 2001). Therefore in this work we consider the evolution of inertia-gravity waves as a basic fluid mechanics problem potentially relevant to all other physical contexts involving motions of rotating density-stratified fluids within a spherical shell. We then apply the findings to the problem of our primary interest – understanding the transformation of oceanic inertia-gravity waves into small vertical and horizontal scales.

Surprisingly, even in the simplest linear setting, such a basic process as evolution of near-inertial waves in a stratified rotating fluid confined between two parallel surfaces is not properly understood. Within the framework of the commonly used model based upon the 'traditional' approximation (i.e. with the horizontal component of the local angular velocity of the Earth being neglected), near-inertial waves of frequency σ propagating on the β-plane polewards have a simple turning point at their inertial latitude ϕ, where σ equals the local Coriolis parameter $f = 2\Omega \sin\phi$, and Ω is the angular frequency of the Earth rotation (LeBlond & Mysak 1978; Munk 1980; Gerkema *et al.* 2008).

Dynamics in a spherical shell is qualitatively different: the meridional eigenfunctions of a motion of frequency σ extend beyond the inertial latitude; this extended part of the eigenfunctions is characterised by a strong decrease of both vertical and horizontal scales (Friedlander & Siegmann 1982; Dintrans, Rieutord & Valdettaro 1999). However, so far the spherical geometry has proved to be difficult for analytic consideration: '*... the problem's variables are not separable, rendering the analysis untractable*' (Dintrans *et al.* 1999). The problem remains challenging to numerics since the numerical studies were confined to the idealised situations of linear buoyancy frequency N profile (Dintrans *et al.* 1999). The analysis of arbitrary stratification profiles carried out by Friedlander & Siegmann (1982) and Friedlander (1982) was aimed at spectral properties of the discrete spectrum and excluded some singular modes. So far none of the approaches tried have captured the aspects of inertia-gravity wave evolution that we are interested in. We will analytically examine wave dynamics in spherical geometry in a separate follow-up paper by extending the approach developed here for the β-plane.

An alternative line of research based on the 'non-traditional' β-plane elucidated the overall qualitative picture of wave evolution for wavepackets, which is practically, and conceptually, more attractive than the use of global meridional eigenfunctions (Gerkema & Shrira 2005*a*, *b*). For near-inertial inertia-gravity waves confined between two horizontal planes on the f-plane, the full account of the Coriolis force changes

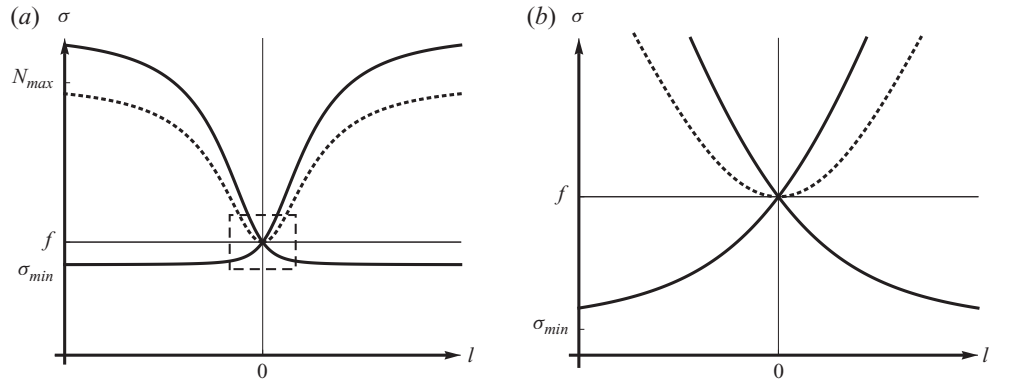

FIGURE 1. (*a*) Sketch of meridional cross-section of dispersion relation $\sigma(l)$. The solid line shows $\sigma(l)$ on the non-traditional f-plane and the dotted line on the traditional f-plane, both for an arbitrary vertical mode, l is the meridional wavenumber; and (*b*) zoomed in vicinity of small l band, N_{max} is the maximal value of buoyancy frequency $N(z)$.

two key features of the dispersion relation, as illustrated in figure 1 for an arbitrary stratification profile provided $N > f$ (for more detail, see Gerkema & Shrira 2005*a*). (i) There appears a new 'subinertial' branch confined to the $O(f/N)^2$ frequency band (σ_{min}, f) which corresponds to waves trapped in the minima of the buoyancy frequency N. (ii) The group velocity at zero wavenumber is finite, with the subinertial branch representing a direct continuation of the superinertial branch. (Note that in the example shown in figure 1 the maximal value of buoyancy frequency N_{max} is chosen to be $2.5f$. This makes the high-frequency extension of the wave existence range look more significant than for more common larger values of N_{max}).

The sketch makes it easy to capture a qualitative picture of a wavepacket's evolution on the 'non-traditional' β-plane. Consider a wavepacket with central frequency σ_0 $(\sigma_0 > f)$ propagating polewards. Its frequency σ_0 remains constant while the local value of f increases. On reaching the inertial latitude, where $f = \sigma_0$, the wave obviously cannot continue its poleward propagation and remain superinertial, i.e. with $\sigma_0 > f$. The wavepacket should either turn back, retaining its superinertial character, or propagate further polewards as the subinertial mode. In fact, both reflection and penetration are taking place simultaneously; the reflection and transmission coefficients were estimated in Gerkema & Shrira (2005*b*). It was found that a substantial part of wave energy propagates further polewards as subinertial waves. A quantitative analytical description of their evolution is the subject of this paper, with the results of Gerkema & Shrira (2005*b*) providing the starting point. The linearised Euler equations were reduced to a single second-order linear partial differential equation of mixed (Tricomi) type, for which no general analytical approach is known (e.g. Tricomi 1954; Duffy 2008). Apart from analysis of particular exact solutions for constant N, the main insight into the character of wave evolution was inferred from the behaviour of characteristics. It is straightforward to find the characteristics which correspond to ray trajectories (Maas & Harlander 2006) and thus get a qualitative idea of wave propagation. Figure 3(*b*) gives a sample picture of the characteristics for an incoming wave of fixed frequency for a typical ocean stratification with $N > f$ everywhere. It shows that waves get trapped in the narrowing waveguides around the local minima of buoyancy frequency N. The picture is generic in the sense that for any smooth profile of stratification it might

differ from the example just by the number and positions of the waveguides. For each waveguide there is a critical latitude ϕ^* beyond which the waves of a chosen frequency σ_0 cannot penetrate. This latitude corresponds to the tipping point of the 'turning surface' separating the hyperbolicity and ellipticity domains. It can be shown that characteristics of the linearised Euler equations for monochromatic waves of frequency σ_0 have point attractors at $\phi = \phi^*$ for waveguides adjacent to the bottom and in its vicinity for all other waveguides. As far as we are aware, it was not known that there might exist attractors lying on the turning surface detached from the boundaries. Note that the general result by Friedlander (1982) that turning surfaces can introduce only removable singularities is confined to the square integrable solutions only and, therefore, does not apply to the continuous spectrum singular solutions we are interested in. The details are discussed in the follow-up paper. Since in the literature there is no universally established terminology and the term critical latitude is also used in different contexts, to exclude controversy we will refer to these latitudes ϕ^* as *tip latitudes*. In the oceanic context the discrepancy between the tip latitudes and the attractor latitudes for the internal waveguides are insignificant in any sense, being a few metres at most. At the tip latitudes the lower bound σ_{min} of the allowed frequency window for internal waves equals the chosen wave frequency, i.e. $\sigma_{min}(\phi^*) = \sigma_0$. The value of σ_{min} depends upon the local Coriolis parameter in such a way that it increases polewards; therefore for any given near-inertial frequency σ_0 there always exists such a latitude. This lower bound also depends upon the local stratification profile and, hence, is different for each of the waveguides. In the vicinity of ϕ^*, the meridional wavenumber tends to infinity and the vertical scale to zero. At the same time, as it is easy to see from figure 1, the wave group velocity tends to zero as $\sigma_{min} \to \sigma_0$, which, along with the narrowing of the waveguides, enhances the wave amplitude.

Although the analysis of characteristics is an excellent tool for getting a qualitative picture it cannot address a number of fundamental questions. Can waves be reflected from the tip latitude ϕ^*? How can the wave evolution be described quantitatively? Waves in nature are never monochromatic; in which way does the evolution of a real finite bandwidth wavepacket differ from that of a monochromatic wave? The vertical focusing of the wave combined with a sharp decrease of the wavelength and group velocity prompted a suggestion that wave breaking and, therefore, enhanced mixing, are a very likely outcome of the evolution (Maas 2001; Gerkema & Shrira 2005*a*, *b*). This hypothesis, based on a preliminary analysis of the linear problem for a monochromatic wave, certainly needs thorough examination. What is the outcome of the evolution of realistic wavepackets, and on what environmental parameters does it depend? The paper aims to address these open questions by studying wave evolution inside the narrowing wedge-like waveguides. Note that to get trapped in these waveguides the waves should not necessarily pass the inertial latitude, as wind-generated inertia-gravity waves propagating downwards (e.g. Pollard & Millard 1970; Van Haren 2006; Danioux & Klein 2008) and waves generated by the bottom topography (e.g. Leaman 1976; Kasahara 2009) as well as by tides through subharmonic parametric resonance could also get trapped inside the narrowing waveguides. Hence, this paper which describes dramatic contraction of wave vertical and horizontal scales, even in an inviscid setting, also contributes to clarifying the unresolved issue of finding mechanisms of the dissipation of inertia-gravity waves.

It is worth noting that the wave attractors encountered while examining the inertia-gravity waves in the ocean represent the basic types of generic attractors for

inertia-gravity waves in a rotating fluid with an arbitrary stable density stratification $N(z)$. Indeed in the vicinity of these attractors because of the shrinking of wave scales the wave evolution is determined by local profile of $N(z)$. Three basic situations characterised by the dominance in the local expansion of $N(z)$ of linear, quadratic and constant terms, respectively, correspond to the three basic types of attractors ('wedge', 'parabolic' and 'corner'.) In this sense the solutions found describing field behaviour in the vicinity of these attractors are universal.

The paper is organised as follows. In §2 we formulate the basic equations on the non-traditional β-plane and set out the problem. In §3, utilising the natural separation of scales, we develop the WKB description and explicitly formulate the conservation of wave action principle, which is valid for all types of internal waves on the 'non-traditional' β-plane. Then we derive explicit analytic solutions describing inviscid evolution of a monochromatic wave inside each of the three basic waveguides. The peculiarity of the problem is that for the wedge waveguides the WKB approximation works progressively better as the wave approaches the attractor latitude; correspondingly, in the limit the solutions describing formation of singularity become exact. In reality waves are not monochromatic, wavepackets always have finite bandwidth, and for each Fourier component, the singularity is located at a different latitude. It is not *a priori* clear whether the packet remains focused or not. This issue is addressed in §4, where an analytical description of the evolution of a packet of finite bandwidth is developed. We show that the packet remains focused. Although the packet spreading due to dispersion slows down the wave amplitude growth, it cannot prevent formation of a singularity at the tipping latitude. That is, the singular focusing is robust. Some implications of the findings, as well as the dependence of wave evolution on density stratification and latitude, are discussed in §5.

2. Setting the problem

We begin with the equations of motion of a rotating density-stratified ideal fluid in the Boussinesq approximation. The notation is standard: $\boldsymbol{u}=(u, v, w)$ is the velocity field, with zonal (u), meridional (v) and radial (w) velocity components, p is the departure of pressure from its hydrostatic value (divided by a constant reference density) and b is the buoyancy:

$$\frac{\mathrm{D}\boldsymbol{u}}{\mathrm{D}t} + 2\boldsymbol{\Omega} \times \boldsymbol{u} + \nabla p - b\boldsymbol{n} = 0, \quad \boldsymbol{n} = (0, 0, 1), \tag{2.1a}$$

$$\nabla \cdot \boldsymbol{u} = 0, \tag{2.1b}$$

$$\frac{\mathrm{D}b}{\mathrm{D}t} + N^2(z)\boldsymbol{u} \cdot \boldsymbol{n} = 0. \tag{2.1c}$$

We use the Cartesian (more precisely pseudo-Cartesian) frame with the horizontal coordinates following the spherical surface: x is zonal (west–east), y is meridional (south–north) and z is the radial or vertical coordinate. We place the origin of the frame $z=0$ at the lower boundary of the spherical shell which is presumed to be flat (e.g. Greenspan 1968; LeBlond & Mysak 1978; Miropol'sky 2001).

In the oceanic context, the motions are confined between the free surface at the top and the solid flat bottom and are subject to standard boundary conditions. At the flat bottom $z=0$ the inviscid no-flux condition requires

$$\boldsymbol{u}(0) \cdot \boldsymbol{n} = w(0) = 0, \tag{2.2}$$

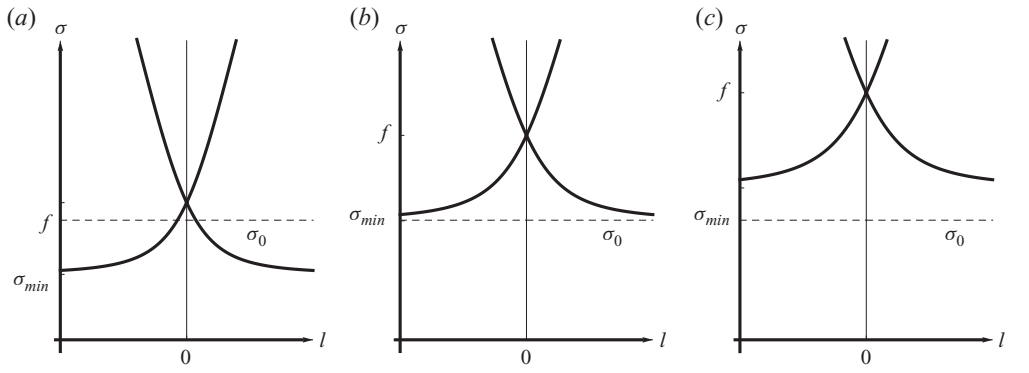

FIGURE 2. Meridional dependence of local dispersion $\sigma(l)$ and evolution of wavenumber l of a wavepacket of a constant frequency σ_0. The initial situation is sketched in (a): there two wavepackets of subinertial wave frequency $\sigma_0 < f$ with wavenumbers $\pm l$ propagate in opposite directions. If we follow the packet moving polewards, its frequency σ_0 remains constant, while the local Coriolis frequency and correspondingly σ_{min} increase, making the wave more and more subinertial until it reaches the stage shown in (b), where $\sigma_{min} \Rightarrow \sigma_0$. The packet of frequency σ_0 cannot penetrate beyond the latitude where $\sigma_{min} = \sigma_0$. Further poleward $\sigma_{min} > \sigma_0$ and, as illustrated in (c), there are no solutions of local dispersion relation for $\sigma = \sigma_0$.

while at the outer surface $z = H$, we adopt the 'rigid lid' approximation, which implies

$$w(H) = 0. \tag{2.3}$$

It is worth noting that for the inviscid motions under consideration the free surface boundary condition is identical to that at the rigid surface. Hence, all the results will also be equally applicable for any rotating stratified fluid confined between two rigid shells.

We will consider wave motions in the linear setting on the non-traditional β-plane. The linearised equations of motions (2.1a)–(2.1c) and the boundary conditions (2.3) and (2.2) can be rewritten as

$$u_t - fv + \tilde{f}w = -p_x, \tag{2.4a}$$

$$v_t + fu = -p_y, \tag{2.4b}$$

$$w_t - \tilde{f}u = -p_z + b, \tag{2.4c}$$

$$u_x + v_y + w_z = 0, \tag{2.4d}$$

$$b_t + N^2(z)w = 0, \tag{2.4e}$$

$$w(0) = w(H) = 0, \tag{2.5}$$

where the Coriolis parameter f varies linearly with the meridional coordinate ($f = f_0 + \beta y$), while $\tilde{f}$ is kept constant to ensure conservation of vorticity and angular momentum (Grimshaw 1975). The parameters $\tilde{f}$, f_0 and β are defined in the usual way:

$$(\tilde{f}, f_0) = 2|\boldsymbol{\Omega}|\,(\cos\phi, \sin\phi), \quad \beta = 2|\boldsymbol{\Omega}|\cos\phi/R,$$

where ϕ denotes a fixed latitude, $\boldsymbol{\Omega}$ denotes the sphere's angular velocity and R denotes the sphere's radius. The buoyancy frequency N is assumed to depend only on the vertical direction, i.e. $N = N(z)$.

Similarly, in the spirit of the qualitative analysis illustrated in figure 2, a straightforward analysis of local dispersion relation for a wave with non-zero zonal

wavenumber propagating polewards on the β-plane could also be carried out (see also Gerkema & Shrira 2005*a*, § 5). As the wave moves polewards and becomes more subinertial it experiences a dramatic increase of the meridional component of the wavevector, while the zonal component retains its initial value. This observation implies that subinertial waves propagating polewards tend towards purely meridional propagation. For simplicity, we confine our consideration to the case of strictly meridional wave propagation, that is we set $\partial_x \equiv 0$. It is then convenient to introduce streamfunction ψ:

$$v = \psi_z, \quad w = -\psi_y. \tag{2.6}$$

It is straightforward to reduce the system (2.4*a*)–(2.4*e*) to a single equation for ψ,

$$\Delta\psi_{tt} + N^2\psi_{yy} + f^2\psi_{zz} + \tilde{f}^2\psi_{yy} + 2f\tilde{f}\psi_{yz} + \beta\tilde{f}\psi_z = 0, \tag{2.7}$$

where the boundary conditions (2.5) take the form

$$\psi_y(0) = \psi_y(H) = 0. \tag{2.8}$$

Our further analysis will be based upon (2.7) with boundary conditions (2.8).

3. Monochromatic wave: WKB description

The basic equation (2.7) admits a Fourier transform with respect to t. In this section we will examine spatial evolution of a single Fourier harmonic $\psi \sim \exp\{-\mathrm{i}\sigma t\}$, and in this sense we will speak about evolution of a monochromatic wave. Fourier transform reduces (2.7) to a mixed (Tricomi)-type second-order PDE with coefficients dependent on both spatial variables. The condition on its hyperbolicity which specifies the domain where the wave can exist is

$$(f\tilde{f})^2 - (N^2 + \tilde{f}^2 - \sigma^2)(f^2 - \sigma^2) > 0. \tag{3.1}$$

For a typical oceanic stratification the hyperbolic and elliptic domains have a fairly complicated geometry illustrated in figure 3 by a thick solid line. Even in the simplest geometry for such a Tricomi-type boundary problem, there is no constructive way of finding a solution (see e.g. Tricomi 1954; Duffy 2008). Fortunately, in nature, there is a wide separation of scales, which we discuss and exploit below to develop an asymptotic WKB description of wave propagation.

In this section, we will focus on the peculiarities of inertia-gravity wave propagation on the non-traditional β-plane. For simplicity, we confine ourselves to the situations with no ambient large-scale oceanic motions, and where the only large-scale cause of inhomogeneity for internal waves is the meridional variation of the Coriolis parameter f. That is, the characteristic length scale of the inhomogeneity, L, is

$$L \sim \frac{f_0}{\beta} = R\tan\phi \sim R. \tag{3.2}$$

Being interested in wave motions of much shorter scales, we introduce a small parameter, ε, to characterise the assumed wide separation of scales between L and the wave motions of characteristic wavenumber $O(l_0)$, as

$$\varepsilon = (l_0 L)^{-1} \ll 1. \tag{3.3}$$

Then, with appropriately scaled independent variables, the explicit β-dependence in (2.7) becomes $O(\varepsilon)$, and we can rewrite the equation in an equivalent form

$$\Delta\psi_{tt} + N^2\psi_{yy} + f(\varepsilon y)^2\psi_{zz} + \tilde{f}^2\psi_{yy} + 2f(\varepsilon y)\tilde{f}\psi_{yz} = -\varepsilon\beta\tilde{f}\psi_z, \tag{3.4}$$

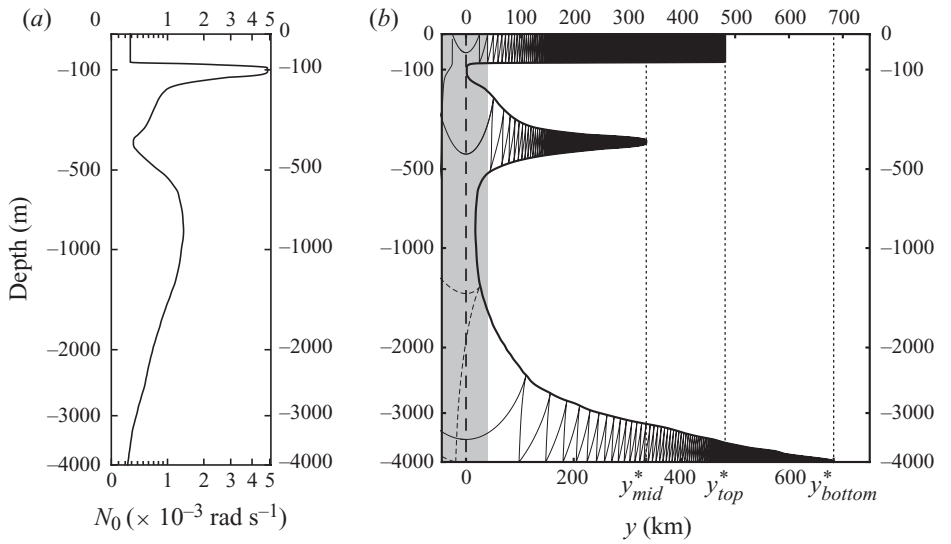

FIGURE 3. (*a*) A typical ocean stratification profile $N(z)$. (*b*) Thick solid line indicates boundary of the hyperbolicity/ellipticity domains for a wave of frequency σ_0. Thick dashed vertical line indicates the inertial latitude, where $\sigma_0 = f$, y is counted from the inertial latitude. Characteristics are shown in thin lines: thin solid, characteristics going through; thin dashed reflected characteristics. Thick dotted lines indicate the positions of the tip latitudes; their coordinates are denoted by y^*. Solution is sought to the right of the grey zone.

which prompts the use of the WKB description. In the limit $\varepsilon \to 0$ we recover the non-traditional f-plane considered in detail by Gerkema & Shrira (2005*a*). In this limit the coefficients of our basic equation (3.4) cease to depend on the meridional coordinate y, which allows Fourier transform with respect to y. The solution for a single Fourier harmonic with meridional wavevector $\boldsymbol{k} = \{0, l\}$ and frequency σ can then be sought in the form $\psi = \Psi(z, l, \sigma) \exp \mathrm{i}(ly - \sigma t)$, which implies

$$l^2(N^2 - \sigma^2 + \tilde{f}^2)\Psi - 2il\tilde{f}f\Psi_z + (\sigma^2 - f^2)\Psi_{zz} = 0, \quad \Psi(0) = \Psi(H) = 0. \tag{3.5}$$

Substituting

$$\Psi(z, l, \sigma) = \Phi(z, l, \sigma)\, \mathrm{e}^{\mathrm{i}\delta z}, \quad \text{where} \quad \delta = \frac{lf\tilde{f}}{(\sigma^2 - f^2)}, \tag{3.6}$$

leads to the following Sturm–Liouville boundary-value problem for Φ:

$$\Phi'' + l^2 \left[\frac{N^2(z) - \sigma^2}{\sigma^2 - f^2} + \left(\frac{\sigma\tilde{f}}{\sigma^2 - f^2} \right)^2 \right] \Phi = 0, \quad \Phi(0) = \Phi(H) = 0. \tag{3.7}$$

This specifies the countable spectrum of eigenvalues l_n^2 as a function of the chosen frequency σ, thus prescribing the dispersion relation $l = l_n(\sigma)$, and the structure of the eigenfunctions $\Phi_n(z)$. Note that both l_n^2 and $\Phi_n(z)$ depend perimetrically on f and therefore through f on y. Hence, the boundary-value problem (3.7) could be viewed as a way to specify meridional dependence of wavenumber l for a given σ and stratification profile $N(z)$. The basic models of stratification relevant to subinertial waveguides were considered by Gerkema & Shrira (2005*a*), and since the corresponding solutions of the boundary-value problem (3.7) will be used throughout this paper, we provide a summary of the necessary results below.

3.1. *Evolution of wavenumber and vertical scale in the basic models*

First, we will look at the dispersion relation and group velocities for the three basic models of waveguides considered by Gerkema & Shrira (2005*a*) and evolution of wavenumber and vertical scale in the vicinity of the corresponding attractors. Since the wave can exist only in regions where the buoyancy frequency is less than that prescribed by the hyperbolicity condition (3.1), waveguides are formed around the minima in $N(z)$, effectively trapping the wave and focusing it towards the minima as waves advance polewards. Figure 3(*a*) shows a typical stratification profile of the ocean, with the three minima where waves can become trapped. The first is in the upper ocean mixed layer at the top, bounded from above by the ocean surface and from below by the seasonal thermocline; the mixed layer creates the 'upper' or 'top' waveguide with typical vertical thickness of $\sim 10^2$ m. In the main body of the ocean, there is another minimum between the seasonal thermocline and the main pycnocline, creating a 'mid-ocean' or 'middle' waveguide of typical thickness $\sim 5 \times 10^2$ m. The deepest minimum is to be found at the ocean floor. This creates the bottom waveguide which is the largest, with thickness $\sim 10^3$ m.

Although, for each of these waveguides, the shape of local variation in N around its minimum is different, which results in asymptotically different dispersion relations, the general feature of all the waveguides is that their thickness gradually decreases with distance from the inertial latitude (see figure 3*b*) except for the constant thickness top waveguide. Each waveguide ends at a certain tipping latitude, where $\sigma_{min} = \sigma$:

$$\sigma_{min}^2 = \tfrac{1}{2}\left(\lambda - [\lambda^2 - (2fN)^2]^{1/2}\right), \quad \lambda = N^2 + f^2 + \tilde{f}^2, \tag{3.8}$$

which corresponds to a distance y^* polewards from the inertial latitude

$$y^\star = \frac{1}{\beta}\left(-f_0 + \sigma\sqrt{\frac{N^2 - \sigma^2 + \tilde{f}}{N^2 - \sigma^2}}\right), \tag{3.9}$$

provided $N^2 > \sigma^2$. Further propagation polewards for waves of the chosen frequency is no longer possible.

3.1.1. *The bottom waveguide: a 'wedge' attractor*

Near the ocean bottom $N^2(z)$ usually varies slowly and attains its minimal value N_0 at the bottom. With good accuracy it can be approximated by the Taylor expansion as $N^2(z) = N_0^2 + \gamma_1 z$ (N_0^2 and $\gamma_1 = N_0^2/h$ are constants, h is the characteristic scale of vertical inhomogeneity). The resulting wedge-shaped hyperbolicity domain confined between the hyperbolicity/ellipticity boundary specified by (3.1) and the horizontal bottom $z = 0$ which hosts the wedge attractor, has nothing specific to the oceanic context. The wedge attractors are generic: it is the interpretation of the results which is context-specific and will be discussed later. The Sturm–Liouville boundary-value problem (3.7) then has solutions in the form

$$\left.\begin{aligned} &\Phi = a_{(\Phi)}\mathrm{Ai}\left(\tilde{l}^{2/3}\left[z - \frac{\Delta}{\gamma_1 C}\right]\right), \quad \tilde{l}^2 = \frac{l^2\gamma_1}{C}, \quad C = f^2 - \sigma^2; \\ &\Delta = (f\tilde{f})^2 - \left(N_0^2 - \sigma^2 + \tilde{f}^2\right)C. \end{aligned}\right\} \tag{3.10}$$

Here $a_{(\Phi)}$ is the amplitude and $\mathrm{Ai}(\xi)$ is the Airy function. Originally, we required Φ to be zero at the bottom ($z = 0$) and at the upper boundary ($z = H$), but to get the solution in the simple form of the Airy function the boundary condition requiring vanishing of Φ has been moved to infinity. Because of the Airy functions' fast decay

outside the waveguide, the error caused by the modification of the boundary is negligible. The corresponding wavenumbers l_n are expressed in terms of zeros of $\mathrm{Ai}(\xi)$ denoted as $-s_n$,

$$l_n = \pm\gamma_1 C^2 \left(\frac{s_n}{\Delta}\right)^{3/2}, \tag{3.11}$$

where s_n are known positive constants ($s_n \approx 2.34,\ 4.09,\ 5.52,\ 6.79, \ldots, (3\pi(4n-1)/8)^{2/3}$; the first term of large n asymptotic expansion for s_n, $s_n = (3\pi(4n-1)/8)^{2/3}$, gives at least 1.8×10^{-2} accuracy for $n \geqslant 1$ and 2.2×10^{-3} for $n \geqslant 4$. Higher-order terms of the expansion are given in Abramowitz & Stegun (1965, § 10.4).

The group velocity is given by

$$\frac{\mathrm{d}\sigma}{\mathrm{d}l} = \frac{\mp\Delta^{5/2}}{\gamma_1\sigma C s_n^{3/2}\left[4\Delta + 3C\left(N_0^2 - \sigma^2 + \tilde{f}^2 + C\right)\right]}. \tag{3.12}$$

In an unspecified vicinity of the singularity the asymptotics in terms of the distance to the singularity $\hat{y}$ take the form

$$l_n(y) \sim \hat{y}^{-3/2}, \quad \frac{\mathrm{d}\sigma}{\mathrm{d}l} \sim \hat{y}^{5/2}. \tag{3.13}$$

The shrinking of the wave field vertical scale is determined by two different factors. The first one is imposed by the eigenfunction $\Phi_n(z)$ specified by (3.10); by virtue of (3.10), (3.13) it decreases as $l^{-2/3}$ or, in terms of $\hat{y}$, as $\hat{y}^1$. The second contribution to the vertical dependence is due to the exponential in the full expression for the solution (3.6) $\psi = \Phi \exp \mathrm{i}(ly - \sigma t + \delta z)$; it is decreasing as δ^{-1} or $\hat{y}^{3/2}$. This factor becomes essential and even dominant only in the vicinity of the singularity.

3.1.2. *The 'mid-ocean' waveguide: 'parabolic' attractor*

Near a generic minimum not adjacent to a boundary, $N(z)$ could be expanded as $N^2(z) = N_0^2 + \gamma_2(z-z_m)^2$, where N_0^2 and $\gamma_2 = N_0^2/h^2$ are constants, and z_m is the position of the chosen local minimum of $N^2(z)$. This creates a parabolic domain around the minimum N_0, imparting the name 'parabolic' attractor. Again, we consider the example in the oceanic context, but all the results obtained here apply to parabolic attractors everywhere as long as the adopted generic expansion of N around z_m remains valid. By changing the origin to the point $z = z_m$ and the boundary conditions to $\Phi \to 0$ as $z = \pm\infty$, the eigenfunctions can be found from (3.7) in the explicit form

$$\Phi = a_{(\Phi)}\mathscr{H}_n(\hat{z})\mathrm{e}^{-\hat{z}^2/2}, \quad \text{where} \quad \hat{z} = \left(\frac{l^2\gamma_2}{f^2-\sigma^2}\right)^{1/4} z, \tag{3.14}$$

where $a_{(\Phi)}$ is the amplitude and $\mathscr{H}_n$ is the nth Hermite polynomial. Again because of the fast $\mathrm{e}^{-\hat{z}^2/2}$ decay outside the waveguide, the error due to moving the boundary conditions to $z = \pm\infty$ proves to be negligible. The explicit dispersion relation was found to be

$$l = \pm(2n+1)\gamma_2^{1/2}\frac{C^{3/2}}{\Delta}, \quad n > 0, \quad C = f^2 - \sigma^2, \quad \Delta = (f\tilde{f})^2 - \left(N_0^2 - \sigma^2 + \tilde{f}^2\right)C, \tag{3.15}$$

which yields the group velocity

$$\frac{\mathrm{d}\sigma}{\mathrm{d}l} = \frac{\mp\Delta^2}{\sigma(\gamma_2 C)^{1/2}(2n+1)\left[3\Delta + 2C\left(N_0^2 - \sigma^2 + \tilde{f}^2 + C\right)\right]}.$$

The asymptotics in terms of the distance $\hat{y}$ to the tipping latitude are given by

$$l_n \sim \hat{y}^{-1}, \quad \frac{\mathrm{d}\sigma}{\mathrm{d}l} \sim \hat{y}^2. \tag{3.16}$$

The eigenfunction wave vertical scale decreases as $l^{-1/2}$ or $\hat{y}^{1/2}$, while the vertical scale due to the exponential decreases as δ^{-1} or $\hat{y}^1$. Again the contribution of the exponential will be dominant near the singularity.

3.1.3. *The upper waveguide: a 'corner' attractor*

In the upper mixed layer of the ocean the buoyancy frequency can be assumed to be constant, that is $N^2(z) = N_c^2$ for $z \geqslant z_m$. This creates an attractor at the bottom corner of the parabolic line (at $z = z_m$), imparting the name 'corner' attractor. While from figure 3(*b*) it is impossible to see that this is indeed a point attractor, it is shown numerically for a model with constant N in Gerkema & Shrira (2005*b*). Hereinafter, we use the terms corner waveguide and upper waveguide interchangeably to emphasise universality of the results. We move the origin of z to z_m and then the eigenfunctions of the boundary-value problem (3.7) can be written as

$$\Phi = a_{(\Phi)} \sin\left(\frac{n\pi z}{H}\right), \quad n \in \mathbb{N}, \tag{3.17}$$

where amplitude $a_{(\Phi)}$ is a real constant. The corresponding dispersion relation reads as

$$l = \frac{\pm n\pi(\sigma^2 - f^2)}{H\sqrt{\Delta}}, \quad \text{where } \Delta(y) = (f(y)^2 - \sigma^2)\left(\sigma^2 - N_0^2\right) + \sigma^2 \tilde{f}^2. \tag{3.18}$$

Note that $l(\sigma)$ has a singularity when $\Delta(y) \to 0$, implying that the wavelength tends to zero as y approaches this point, which we denote as y^*, or in terms of latitude as ϕ^*. The group velocity is given by

$$\frac{\mathrm{d}\sigma}{\mathrm{d}l} = \frac{\pm H\Delta^{3/2}}{n\pi\sigma(\Delta + f^2\tilde{f}^2 + (\sigma^2 - f^2)^2).} \tag{3.19}$$

The asymptotics in terms of the distance to the singularity $\hat{y} \equiv y - y^*$ are

$$l \sim \hat{y}^{-1/2}, \quad \frac{\mathrm{d}\sigma}{\mathrm{d}l} \sim \hat{y}^{3/2}. \tag{3.20}$$

Due to the idealisation adopted in this very particular model of stratification, the width of the waveguide and the vertical scale of the eigenfunctions $\Phi_n(z)$ remain constant. Correspondingly, the characteristic vertical scale of all wave-induced physical quantities, such as velocity components, shear, etc., is decreasing entirely due to the exponential factor $\mathrm{e}^{\mathrm{i}\delta z}$ as δ^{-1} or, in terms of the distance to singularity in its vicinity, as $\hat{y}^{1/2}$.

3.2. *Evolution of wave amplitude*

With ε small but non-zero the coefficients in (3.4) vary slowly with y and there is an additional term compared with the f-plane. Since there is no method for solving such mixed-type problems (3.4) and (2.8) in a general setting, we exploit the already discussed smallness of ε and apply the WKB asymptotic expansion (e.g. Fedoryuk 1993; Miropol'sky 2001). For the situations where a single vertical mode specified by the chosen mode number n is dominant, the expansion takes the form

$$\psi = \Psi_{n(0)}(z, \varepsilon y) \exp \mathrm{i}\left[\int_{y_i}^{y} l_n(\varepsilon y_1)\,\mathrm{d}y_1 - \sigma t\right] + \sum_{m,s=1} \varepsilon^m \psi_{s(m)}(z, \varepsilon y), \tag{3.21}$$

where y_i is the initial position of the wavepacket. The mth-order corrections in ε denoted as $\psi_{s(m)}(z, \varepsilon y)$, which are not confined to the initially chosen nth mode, are usually used only to check the accuracy of the leading-order terms. The chosen mode number n is included in the s summation index. Note that it is possible to consider a more general problem, where in the zeroth order we begin with a number of wavepackets belonging to different modes. In our context, analysis of such situations does not promise a new insight and, therefore, lies beyond the scope of the present paper. A detailed description of the WKB procedure for multi-modal systems in the context of internal waves could be found in, for example, Miropol'sky (2001).

Substituting (3.21) into (3.4) yields in the zeroth order in ε the same boundary value problem (3.7), thus the same dispersion relation and group velocity formulae still apply. In the first order in ε, we find (with the mode number subscript dropped)

$$l^2(N^2-\sigma^2+\tilde{f}^2)\Psi_{(1)}-2\mathrm{i}lf\tilde{f}\partial_z\Psi_{(1)}+(\sigma^2-f^2)\partial_{zz}^2\Psi_{(1)}=F[\Psi_{(0)}],\quad \Psi_{(1)}(0)=\Psi_{(1)}(H)=0, \tag{3.22}$$

where

$$F\left[\Psi_{(0)}\right]=\tilde{f}\partial_y f\partial_z\Psi_{(0)}+(N^2-\sigma^2+\tilde{f}^2)(2\mathrm{i}l\partial_y\Psi_{(0)}+\mathrm{i}\Psi_{(0)}\partial_y l)+2f\tilde{f}\partial_{yz}^2\Psi_{(0)}. \tag{3.23}$$

The requirement of solvability of (3.22) imposes the following orthogonality condition:

$$\int_0^H F\left[\Psi_{(0)}\right]\Psi_{(0)}^*\,\mathrm{d}z=0,\quad \int_0^H \left(F\left[\Psi_{(0)}\right]\right)^*\Psi_{(0)}\,\mathrm{d}z=0, \tag{3.24}$$

where $*$ denotes the complex conjugate. Combining these two conditions we find

$$\int_0^H [2\tilde{f}f_y\Psi^*\Psi_z+(N^2-\sigma^2+\tilde{f}^2)(2\mathrm{i}l\partial_y(\Psi\Psi^*)+2\mathrm{i}\Psi\Psi^* l_y)+2f\tilde{f}(\Psi_z\Psi_y^*-\Psi_z^*\Psi_y)]\,\mathrm{d}z=0, \tag{3.25}$$

where $\Psi=\Psi_{(0)}$. Then using the substitution $\Psi(z,l,\sigma)=\Phi(z,l,\sigma)\exp\mathrm{i}(\delta z)$ we get the conservation law

$$\frac{\partial}{\partial y}\left[l\int_0^H(N^2-\sigma^2+\tilde{f}^2)\Phi^2\,\mathrm{d}z+f\tilde{f}\delta\int_0^H\Phi^2\,\mathrm{d}z\right]=0, \tag{3.26}$$

which prescribes the evolution of the wave amplitude. Equation (3.26) is the stationary form of the conservation of wave action equation, the quantity in square brackets is the wave action flux (Whitham 1974). As far as we are aware, the conservation of wave action has never been deduced for internal wave motions on the non-traditional β-plane. The conservation of wave action equation in the stationary form (3.26) describes the evolution of wave amplitude of a narrowband wavepacket of frequency σ as it propagates through inhomogeneity created by the latitude-dependent rotation. The wave belongs to a particular nth mode implicitly specified by the presence of wavenumber l in (3.26); l satisfies the dispersion relation provided by the boundary-value problem (3.22).

The equation, in general, is applicable to all internal wave motions, although the non-traditional effects are more prominent for the near-inertial waves we are focusing on. The change in energy of propagating waves could be interpreted in two different ways. In the terrestrial frames of reference (e.g Cartesian frame and the β-plane or spherical coordinates), the wave propagates through the steady spatial inhomogeneity created by the latitude-dependent rotation. Since such frames are not inertial, there is no special reason for the energy of the wavepacket to be conserved. If we consider the problem in an inertial frame, then we arrive at the situation similar to the classical

examples of waves propagating on non-uniform currents: in our case waves propagate through inhomogeneous flow created by the sphere's solid-body rotation.

Explicitly defining the amplitude in terms of the streamfunction $\Phi(z) = a_{(\Phi)}\tilde{\Phi}(z)$, where $\tilde{\Phi}(z)$ is a eigenfunction of (3.7) depending upon the waveguide, we obtain

$$a_{(\Phi)} = a_0 \left(\int_0^H [l(N^2 - \sigma^2 + \tilde{f}^2) + f\tilde{f}\delta]\tilde{\Phi}^2 \, \mathrm{d}z \right)^{-1/2}, \tag{3.27}$$

where a_0 is a constant found by matching with the initial amplitude. The amplitude depends on y through $f(y)$, $l(y)$ and $\tilde{\Phi}^2(y)$. Setting $N^2(z) = N_0^2 + \tilde{N}^2(z)$ we can simplify this to

$$a_{(\Phi)} = a_0 \left\{ \int_0^H \left[\frac{\Delta}{\sigma^2 - f^2} + \tilde{N}^2(z) \right] l\Phi^2 \, \mathrm{d}z \right\}^{-1/2}. \tag{3.28}$$

The evolution of the wave amplitude is specific to each of the three basic waveguides and has to be examined separately for each case.

3.2.1. *The bottom ('wedge') waveguide*

From (3.27), the amplitude's spatial dependence for the bottom waveguide is given by

$$a_{(\Phi)} = a_0 \left(\int_0^\infty \left[l\left(N_0^2 - \sigma^2 + \tilde{f}^2\right) + f\tilde{f}\delta + l\gamma_1 z \right] \left\{ \mathrm{Ai}\left(\tilde{l}^{2/3} \left[z - \frac{\Delta}{\gamma_1 C} \right] \right) \right\}^2 \mathrm{d}z \right)^{-1/2}, \tag{3.29}$$

where $\tilde{l}^2 = l^2\gamma_1/C$ with $l(y)$ being prescribed by (3.11). The expression can be further simplified:

$$a_{(\Phi)} = a_0 \left(\tilde{l}^{-2/3} \int_0^\infty \left[l\left(N_0^2 - \sigma^2 + \tilde{f}^2\right) + f\tilde{f}\delta + \tilde{l}^{-2/3} l\gamma_1 z \right] \mathrm{Ai}(z - s_n)^2 \, \mathrm{d}z \right)^{-1/2}. \tag{3.30}$$

In terms of large l or, equivalently, small distance $\hat{y}$ to the attractor latitude, the leading-order asymptotics are

$$a_{(\Phi)} \simeq \alpha_l \cdot l^{1/6} \simeq \alpha_{\hat{y}} \cdot \hat{y}^{-1/4}, \tag{3.31}$$

where expressions for the constants α_l, $\alpha_{\hat{y}}$ are given in Appendix A. From the Euler equations (2.4*a*)–(2.4*e*) the asymptotics for the other variables follow:

$$a_{(w)} \sim a_{(v)} \sim a_{(u)} \sim a_{(b)} \sim \hat{y}^{-7/4}. \tag{3.32}$$

In the immediate vicinity of the zeros of the eigenfunctions the field variables have different asymptotics, since only the derivatives of the eigenfunction are non-zero. For the nth mode there will always exist n zeros. One is imposed by the boundary condition at the bottom, $\Phi(0) = a_{(\Phi)}\mathrm{Ai}(-s_n) = 0$. The other $n - 1$ occur when the argument of the Airy function passes through the other zeros: s_m, $0 < m < n$. In the immediate vicinity of these zeros the next order in the asymptotics has to be used:

$$a_{(v)} \sim a_{(u)} \sim \hat{y}^{-5/4}, \quad a_{(w)} \sim a_{(b)} \sim 0. \tag{3.33}$$

Hereinafter, for brevity we will often refer to the asymptotics in the vicinity of a zero of the eigenfunction as 'near-zero' asymptotics and those away from a zero of the eigenfunction as 'generic' asymptotics. The Richardson number Ri decreases more

rapidly outside the vicinity of the zeros,

$$Ri = \frac{N^2}{u_z^2 + v_z^2} \sim \hat{y}^{13/2}\,(\text{generic}) \quad \text{and} \quad Ri \sim \hat{y}^{11/2}\,(\text{near-zero}). \tag{3.34}$$

The derivation of the asymptotics for the shear is given in Appendix B.2. The nonlinearity (wave steepness) parameter ε_N (defined as the ratio of amplitude of meridional velocity to the phase velocity) grows more rapidly far from zeros than in their vicinity:

$$\varepsilon_N \sim \hat{y}^{-13/4}\,(\text{generic}), \quad \varepsilon_N \sim \hat{y}^{-11/4}\,(\text{near-zero}). \tag{3.35}$$

Small y asymptotics, which might be of practical interest, are given in Appendix A.

3.2.2. *The 'mid-ocean' ('parabolic') waveguide*

For the mid-ocean waveguide substituting explicit normalised eigenfunctions $\hat{\Phi} = \mathscr{H}_n(\hat{z}) \cdot \mathrm{e}^{-\hat{z}^2/2}$, where $\hat{z} = (l^2\gamma_2/(f^2 - \sigma^2))^{1/4} z \equiv z/b$, into (3.27) we find

$$a_{(\Phi)} = \frac{a_0}{\sqrt{\displaystyle\int_{-\infty}^{\infty} b\left[l\left(N_0^2 - \sigma^2 + \tilde{f}^2\right) + f\tilde{f}\delta + lb^2\gamma_2\hat{z}^2\right]\left\{\mathscr{H}_n(\hat{z})\exp\left(-\frac{\hat{z}^2}{2}\right)\right\}^2 \mathrm{d}\hat{z}}}, \tag{3.36}$$

where $l(y)$ is given by (3.15). The leading-order asymptotics takes the form

$$a_{(\Phi)} \simeq \alpha_l \cdot l^{1/4} \simeq \alpha_{\hat{y}} \cdot \hat{y}^{-1/4}, \tag{3.37}$$

where α_l and $\alpha_{\hat{y}}$ are given in Appendix A, while the asymptotics for other variables are in § 4.3. Small y asymptotics are also available in Appendix A.

3.2.3. *The 'top' ('corner') waveguide*

Similarly, for the upper or top waveguide the amplitude is given by

$$a_{(\Phi)} = a_0 \left(\int_0^H \left[l\left(N_0^2 - \sigma^2 + \tilde{f}^2\right) + f\tilde{f}\delta\right] \sin^2\left(\frac{n\pi z}{H}\right) \mathrm{d}z\right)^{-1/2}. \tag{3.38}$$

Remarkably the expression has the same leading-order asymptotics in $\hat{y}$ as in the case of the bottom and mid-ocean waveguides

$$a_{(\Phi)} \simeq \alpha_l \cdot l^{1/2} \simeq \alpha_{\hat{y}} \cdot \hat{y}^{-1/4}. \tag{3.39}$$

Whether this is just a coincidence or there are deep underlying reasons behind this universality is not clear. The coefficients α_l, $\alpha_{\hat{y}}$ are given in Appendix A along with small y asymptotics.

In all models of stratification considered, the velocity components as well as the inverse Richardson number and nonlinearity monotonously grow and tend to infinity at the tipping latitude. Note that the inverse Richardson number always grows more rapidly than the nonlinearity.

3.3. *Accuracy and range of validity of the asymptotics*

The advantages of using, wherever possible, simple asymptotic solutions for the amplitudes of the previous section, compared to the full formulae (3.30), (3.36) and (3.38), are obvious; we could expect these asymptotics to be valid in a certain unspecified neighbourhood of the singular point for the bottom and middle waveguides. However, it is not *a priori* clear how well they describe the full solution and, crucially, what is their range of validity. Remarkably, for the streamfunction amplitude a_Φ the discrepancy between the full expressions and their small $\hat{y}$

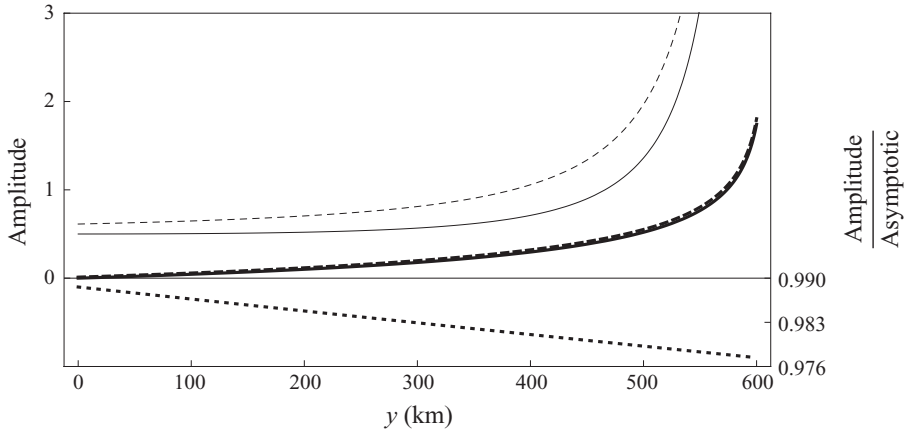

FIGURE 4. Validity of small $\hat{y}$ asymptotics. Evolution of scaled a_Φ is shown in thick lines: thick dashed, a_Φ small $\hat{y}$ asymptotics (3.31); thick solid, a_Φ according to the full formula (3.30); thick dotted, ratio of a_Φ (3.30) to its asymptotics (3.31). Evolution of scaled $l(y)$ is shown by thin lines: solid, $l(y)$ according to (3.11); dashed, asymptotics (3.13), both shifted vertically by 1/2. Parameters used: $N_0 = 2.5 \times 10^{-4}$ s^{-1}, latitude $= 45°$, $\gamma_1 = 4 \times 10^{-10}$ m^{-1} s^{-2}, $a_0 = 5.14 \times 10^{-3}$. The starting point $y = y_{start} = 11$ km is chosen to ensure that the separation of scales condition (3.3) holds for $y \geqslant y_{start}$.

asymptotics is negligible over the entire range of $\hat{y}$ for all models of stratification. This point is demonstrated in figure 4 for the bottom waveguide: evolution of the streamfunction amplitude a_Φ according to the full formula (3.10) and (3.30) is shown and compared to its leading-order asymptotics. This excellent agreement allows us to use the asymptotics as a very good approximation of true dependencies for all $\hat{y}$ throughout the subsequent sections. Note that for other wave characteristics the agreement between the full expressions and their small $\hat{y}$ asymptotics is good but not as spectacularly good as for a_Φ. This point is illustrated in figure 4 by plotting wavenumber dependence $l(y)$ as given by (3.11) and its asymptotic counterpart (3.13).

3.4. *Validity of the WKB solutions*

The WKB expansion is based on the assumption of separation of scales given in (3.3). If the condition is satisfied initially, and as long as we are interested in subinertial waves propagating towards their tipping latitude, which is the case, the wavelength decreases for all the waveguides as specified by their asymptotics; hence the condition of scale separation works progressively better. The most restrictive in our context is the condition that in the process of evolution the wavelength should also remain small compared to the distance to the singular point, $\hat{y}$, that is, the condition

$$l\hat{y} \gg 1 \tag{3.40}$$

has to be satisfied. For the top, middle and bottom waveguides, $l\hat{y}$ evolves by virtue of their asymptotics as $\hat{y}^{1/2}$, $\hat{y}^0$ and $\hat{y}^{-1/2}$, respectively. Each case has to be considered separately.

The bottom waveguide has the asymptotics $\hat{y}^{-1/2}$, implying that as the wave approaches the singularity the condition becomes better satisfied. Hence, since the small parameter ε representing the separation of scales also tends to zero in the limit

$\hat{y} \to 0$, the solution in the form

$$\left.\begin{aligned} &\Phi = b_1 \cdot \hat{y}^{-1/4} \mathrm{Ai}[b_2 \cdot \hat{y}^{-1} z - s_n], \quad b_1 = \text{const.}, \\ &b_2 = |b_l|^{2/3} \left(\frac{\gamma_1}{2 f_0 \beta y^\star} \right)^{1/3}, \quad b_l = -\frac{2\gamma_1 f_0 \beta y^\star s_n^{3/2}}{\bar{\Delta}}, \quad \bar{\Delta} = (2 f_0 \beta + 2\beta^2 y^\star)(N_0^2 - \sigma^2) \end{aligned}\right\} \tag{3.41}$$

tends to the exact solution. Here $y^\star$ is the length of the waveguide specified by (3.9). To return to original physical variables, say velocities, we have to take into account the factor $\mathrm{e}^{\mathrm{i}\delta z}$ eliminated by transformation (3.6).

For the parabolic waveguide, $l\hat{y}$ is monotonically increasing and tends to a finite non-zero value at the singularity. Provided the validity condition (3.40) is satisfied at any chosen initial point, it remains valid at the singularity. This implies that the solution

$$\left.\begin{aligned} &\Phi = m_1 \cdot \hat{y}^{-1/4} \mathscr{H}_n \left[m_2 \frac{z}{\hat{y}^{1/2}} \right] \exp\left(- \left(m_2 \frac{z}{\hat{y}^{1/2}} \right)^2 \Big/ 2 \right), \quad m_1 = \text{const.}, \\ &m_2 = \left(\frac{\gamma_2 |m_l|}{2 f_0 \beta y^\star} \right)^{1/4}, \quad m_l = -\frac{(2n+1)\sqrt{\gamma_2}(2 f_0 \beta y^\star)^{3/2}}{\bar{\Delta}} \end{aligned}\right\} \tag{3.42}$$

is at least $O(\varepsilon)$ accurate when $\hat{y} \to 0$. On the other hand, as $\hat{y} \to 0$ the slope of the turning surface delineating the hyperbolicity/ellipticity domains inevitably becomes supercritical for the characteristics, which results in the characteristics attractor occurring at some $y_{attractor} < y^*$. Therefore, for the parabolic waveguides, it is difficult to expect the WKB to be valid for $y_{attractor} < y < y^*$. Nevertheless the direct substitution of the WKB solution (3.42) into the original streamfunction equation (3.4) and numerical evaluation of the discrepancy shows that the asymptotic solution does satisfy the equation with good accuracy even when $\hat{y} \to 0$. Although for the typical oceanic conditions the interval $|y_{attractor} - y^*|$ is of the order of a few metres at most, the discrepancy might be of significance in other physical contexts. The issue needs further investigation.

For the top waveguide, the asymptotics $l\hat{y} \sim \hat{y}^{1/2}$ implies that the WKB ceases to be valid near the singularity. However, for realistic values of parameters the region of the WKB validity covers almost the entire domain. (The WKB breaks down at $\hat{y} \sim 1m$ with the domain being several hundred kilometres.) We do not elaborate this point here, since, as we show in a separate paper, if viscosity is taken into account then a wavepacket will totally dissipate well before it could leave the domain of the WKB validity. Also the idealisation of sharp interface certainly loses its validity for sufficiently small wavelengths. It is also worth noting that this most idealised model of ocean stratification does not fully capture the true behaviour of the wave field near singularity in the WKB description and therefore, from a mathematical viewpoint, is more challenging than more realistic models. Obviously the WKB description is not applicable in the vicinity of the inertial latitude: it becomes valid for $y > y_{start}$, and y_{start} depends both on stratification and latitude. For the parameters illustrated in figure 4 y_{start} is 11 km. Further on throughout the paper, for consistency we set $y_{start} = 11$ km for all $N(z)$ and all latitudes.

4. Evolution of a finite bandwidth packet

4.1. *Description of finite bandwidth packets*

In the previous section, the wavepacket was assumed to be quasi-monochromatic; however, in reality the wavepackets always have a finite bandwidth. Therefore, although the conclusions of § 3 regarding the existence of a singularity and the behaviour of the wave as it approaches it are valid for each Fourier harmonic, and the problem is linear, we cannot make any conclusions on the behaviour of the packet as a whole. Because for each Fourier component the singularity is located in a different position, it is not *a priori* clear whether the packet remains focused. To address this issue, we consider a packet of finite bandwidth, adopting the approach used in Gnevyshev & Shrira (1989).

Consider a packet with central frequency σ_0 and a characteristic bandwidth $\Delta\sigma$. Assume for certainty its spectrum is Gaussian. Then, starting with (3.21), without loss of generality the streamfunction could be written as

$$\psi(y,z,t)=\frac{1}{\Delta\sigma\sqrt{\pi}}\int_{-\infty}^{\infty}\Psi(y,z,\sigma)\exp\left(\mathrm{i}\int_{y_i}^{y}l(y_1,\sigma)\,\mathrm{d}y_1-\mathrm{i}\sigma t-\left(\frac{\sigma-\sigma_0}{\Delta\sigma}\right)^2\right)\mathrm{d}\sigma, \tag{4.1}$$

where $\Psi(y,z,\sigma)$ and $l(y,\sigma)$ are given by the solution for monochromatic wave discussed in § 3 and here presumed to be known for each σ. Assume that the width of the packet is small compared to the central frequency, i.e. $\Delta\sigma\ll\sigma_0$. Then taking $\sigma=\sigma_0+\tilde{\sigma}$, where $\tilde{\sigma}$ is comparatively small, we expand both l and Ψ in the Taylor series in $\tilde{\sigma}$ around σ_0:

$$\psi=\frac{1}{\Delta\sigma\sqrt{\pi}}\int_{-\infty}^{\infty}[\Psi(y,z,\sigma_0)+\Psi'(y,z,\sigma_0)\tilde{\sigma}+\cdots]$$
$$\times\exp\left[-\sigma_0 t-\mathrm{i}\tilde{\sigma}t+\mathrm{i}\int_{y_i}^{y}[l(y_1,\sigma_0)+l'(y_1,\sigma_0)\tilde{\sigma}+\cdots]\,\mathrm{d}y_1-\left(\frac{\tilde{\sigma}}{\Delta\sigma}\right)^2\right]\mathrm{d}\sigma. \tag{4.2}$$

In this section, we are only concerned with the effects of wavepacket spreading. To assess whether the packet contracts as it approaches the critical point and to find the effect this has on its amplitude, we need to retain only the leading-order ψ term, as the higher-order terms there do not contribute to the packet spreading.

4.2. *First-order approximation*

First, on retaining only the leading-order term in the exponent expansion, we find

$$\psi=\Psi(y,z,\sigma_0)\exp\left[\mathrm{i}\int_{y_i}^{y}l(y_1,\sigma_0)\,\mathrm{d}y_1-\mathrm{i}\sigma_0 t-s^2\right], \tag{4.3}$$

$$\text{where}\quad s=\frac{\Delta\sigma}{2}\left(-t+\int_{y_i}^{y}\frac{\mathrm{d}y_1}{c_g(y_1,\sigma_0)}\right),\qquad c_g=\frac{\mathrm{d}\sigma}{\mathrm{d}l}\ \text{is the group velocity.}$$

It is easy to see that the decay of the wave field, due to distancing of the 'observation point' $y(t)$ from the centre of the wavepacket $y_c(t)$, is given by $\exp(-s^2)$. At $t=0$, the centre of the wavepacket is assumed to be at the position y_i. Then for all times t ($t>0$) the new position of the centre, $y_c(t)$, is prescribed by

$$t=\int_{y_i}^{y_c}\frac{\mathrm{d}y_1}{c_g(y_1,\sigma_0)}, \tag{4.4}$$

and the expression for s can be rewritten as

$$s = \frac{\Delta\sigma}{2}\left(-\int_{y_i}^{y_c}\frac{\mathrm{d}y_1}{c_g(y_1,\sigma_0)}+\int_{y_i}^{y}\frac{\mathrm{d}y_1}{c_g(y_1,\sigma_0)}\right)=\frac{\Delta\sigma}{2}\left(\int_{y_c}^{y}\frac{\mathrm{d}y_1}{c_g(y_1,\sigma_0)}\right). \tag{4.5}$$

We define the meridional scale of the packet L_y as the scale of the field's e-fold decay from the centre of the packet to its periphery. More precisely, L_y is the distance between a 'boundary' point in the packet and its centre, $L_y = |y_b - y_c|$, with y_b specified by the e-fold decay condition $s^2 = 1$.

In the vicinity of the critical latitude for the considered models of waveguides, the group velocity tends to zero with the distance to the singularity $\hat{y}$. Consider the general setting

$$c_g = \alpha\hat{y}^q \quad (q > 1), \tag{4.6}$$

where $\hat{y} = y^\star - y$ is the distance from the point y to the critical point $y^\star$. The condition $s^2 = 1$ applied to (4.5) specifies the evolution of the packet boundary:

$$\hat{y}_b = \hat{y}_c(1 \pm W)^{1/(1-q)}, \quad W = \frac{2\alpha(q-1)\hat{y}_c^{q-1}}{\Delta\sigma}. \tag{4.7}$$

Then the meridional scale of the packet evolves as

$$L_y = |1-(1\pm W)^{1/(1-q)}|\hat{y}_c. \tag{4.8}$$

Since $q > 1$ and $\hat{y}_c \to 0$, it follows that $W \ll 1$, which enables us to simplify the expression for the packet scale:

$$L_y \approx \frac{2\alpha}{\Delta\sigma}\hat{y}_c^q. \tag{4.9}$$

Hence as long as $q > 1$ the wavepacket is always narrowing. For the considered specific models of the bottom, middle and top waveguides, $q = 5/3; 2; 3/2$, correspondingly, the meridional scale decreases as $\hat{y}_c^{5/3}$, $\hat{y}_c^2$ and $\hat{y}_c^{3/2}$, respectively.

4.3. *Second-order approximation*

On taking into account the $O(\sigma-\sigma_0)^2$ term in the expansion of the exponent in (4.2), we find

$$\psi(y,z,t) = \frac{\Psi(y,z,\sigma_0)}{\sqrt{1-\mathrm{i}\mu}}\exp\left[\mathrm{i}\int_{y_i}^{y} l(y_1,\sigma_0)\,\mathrm{d}y_1 - \mathrm{i}\sigma_0 t - \frac{s^2(1+\mathrm{i}\mu)}{1+\mu^2}\right], \tag{4.10}$$

where

$$\mu = \frac{\Delta\sigma^2}{2}\int_{y_i}^{y}\frac{\partial^2}{\partial\sigma^2}l(y_1,\sigma_0)\,\mathrm{d}y_1. \tag{4.11}$$

Therefore, to second order, the spatial decay of the wavepacket is given by the factor $\exp(-s^2/(1+\mu^2))$. As before we define the meridional scale of the packet L_y by the e-fold decay condition, which now takes the form: $s^2/(1+\mu^2) = 1$. For waves in the vicinity of the critical latitude, with the power-like asymptotics

$$l = \alpha_l\hat{y}^p, \quad c_g = \alpha_{c_g}\hat{y}^q (p > 0,\ q > 1), \tag{4.12}$$

it is straightforward to find

$$\mu = \frac{\Delta\sigma^2 q\alpha_l^{(q/p-1)}}{2p\alpha_{c_g}^2(p+2q-1)}\left(\hat{y}^{-(p+2q-1)} - \hat{y}_i^{-(p+2q-1)}\right) \tag{4.13}$$

Since $p+2q-1>1$, in the vicinity of the critical point $\mu\sim\hat{y}^{-(p+2q-1)}$ and, correspondingly, $\mu\gg1$. There could exist interesting intermediate asymptotics in the range $\mu\sim1$; however, we are primarily concerned with the large time limit, and therefore confine our consideration to the situation where $\mu\gg1$. The condition $s^2/\mu^2=1$ specifies $\hat{y}_b$:

$$\pm\frac{\Delta\sigma q(q-1)\alpha_l^{(q/p-1)}}{p\alpha_{c_g}(p+2q-1)}\left(\hat{y}_c^{q-1}-\hat{y}_c^{q-1}\left(\frac{\hat{y}_b}{\hat{y}_i}\right)^{p+2q-1}\right)=\hat{y}_b^{p+q}\hat{y}_c^{q-1}-\hat{y}_b^{p+2q-1}. \tag{4.14}$$

Since $p+2q-1>0$ and $\hat{y}_b\ll\hat{y}_i$, from (4.14) it follows that $\hat{y}_b\to0$ as $\hat{y}_c^{(q-1)/(p+2q-1)}$. Thus, for all three waveguides, the packet remains focused at the critical point for the central harmonic. The finite bandwidth effect noticeably slows down the wave amplitude growth through a factor $\sqrt{2/\mu}\sim\hat{y}^{(p+2q-1)/2}$ due to the $(1-\mathrm{i}\mu)^{-1/2}$ term in (4.14). For each of the waveguides this effect turns the amplitude growth into decay for ψ. The rate of amplitude decay in the bottom, middle and top waveguides is $\hat{y}$, $\hat{y}^{3/4}$ and $\hat{y}^{1/2}$, respectively. However, it is only for ψ that the growth turns into decay. The velocities, vertical shear and the nonlinearity are either stationary or continue to grow, albeit more slowly.

4.4. *Summary*

Here we summarise our main findings on the evolution of subinertial wavepackets propagating polewards in each of the three basic types of waveguides in the rotating stratified fluid on the non-traditional β-plane. As tracing of the characteristics of the basic equation (2.7) suggests (see figure 3), for each waveguide there exists a critical point y^* – the tipping latitude – beyond which a trapped wavepacket cannot propagate. Dependence of y^* on the stratification profile and latitude is given by (3.9). Our key observation is that evolution of wave packets is well described by the WKB. For the bottom and middle waveguides the WKB becomes more accurate as a packet approaches its critical point y^*. Narrowing of the waveguide height down to zero at the critical point and the decrease of the wavepacket group velocity (also down to zero at $y=y^*$) always results in a monotonic growth of the monochromatic wave amplitude (see (3.38), (3.41), (3.42) and figure 4), tending to a singularity at $y=y^*$. This focusing always overcomes the dispersion spreading for finite bandwidth packets (checked to second order) in the sense that the packet remains localised, but the dispersion weakens the amplitude growth and even turns it into decay in terms of ψ for the waveguides considered here.

First, recall that the wave field in terms of the streamfunction is described either by

$$\psi(y,z,t)=\Phi(z)\exp\mathrm{i}(ly-\sigma t+\delta z),\quad \delta=\frac{lf\tilde{f}}{(\sigma^2-f^2)} \tag{4.15}$$

for monochromatic wavepackets, or by a Fourier integral for the packets of finite bandwidth $\Delta\sigma$:

$$\psi(y,z,t)=\frac{1}{\Delta\sigma\sqrt{\pi}}\int_{-\infty}^{\infty}\Psi(y,z,\sigma)\exp\left(\mathrm{i}\int_{y_i}^{y}l(y_1,\sigma)\,\mathrm{d}y_1-\mathrm{i}\sigma t-\left(\frac{\sigma-\sigma_0}{\Delta\sigma}\right)^2\right)\mathrm{d}\sigma. \tag{4.16}$$

4.4.1. *Pattern of evolution*

The derived formulae contain all the information on wave evolution in a somewhat implicit form. To translate the formulae in terms of ψ and Ψ into dependencies of physical quantities of prime interest, and to provide a broad picture of wave evolution, we illustrate and briefly discuss it separately for each waveguide. We plot dependence

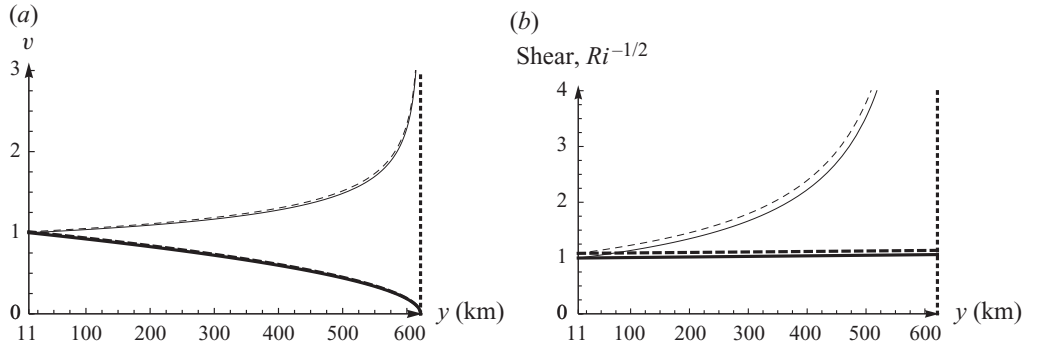

FIGURE 5. Top waveguide: meridional velocity (a) and the vertical shear or $Ri^{-1/2}$ (b). Solid lines represent the full WKB results, dashed lines show their small $\hat{y}$ asymptotics. Evolution of monochromatic wave is plotted in thin lines. Finite bandwidth results are shown in thick lines. The curves for the vertical shear and $Ri^{-1/2}$ are identical. The dotted vertical line near the critical point indicates where the WKB ceases to be applicable as condition (3.40) breaks down. The curves are normalised by choosing a_0 such that the full WKB expressions (solid line) equal one at the chosen starting point y_{start}. Parameters used: $z = z_m$, $y_{start} = 11$ km, $\phi = 45°$, $N_0 = 2.5 \times 10^{-4}$ s^{-1}, $h = 100$ m.

on y of meridional velocity v and full vertical shear $(v_z^2 + u_z^2)^{1/2}$ over the whole range of existence of the subinertial modes. The normalised curves for the vertical shear and $Ri^{-1/2}$ are identical. Dependence of the zonal component u is practically identical to that of v.

Figure 5 illustrates the key features of wave evolution in the top waveguide. It demonstrates that simple asymptotic formulae agree very well with the full WKB results. It should be noted that in this figure all the dependencies are taken at the lower boundary, that is, at the zero of the eigenfunction. Away from zeros the physical quantities increase more rapidly. For the top waveguide the WKB itself ceases to be applicable at a certain distance before the singularity, but in the oceanographic context the distance, being less than a metre for the typical parameters, is negligible for any practical consideration. Therefore the challenging mathematical problem of describing the field in the vicinity of singularity has not been considered here, some analytical results could be found in Gerkema & Shrira (2005*b*). The account of the finite bandwidth of the packet leads to quite dramatic consequences in this case: in the vicinity of eigenfunction zeros the unlimited power growth of the velocities and shear turns into the decay of velocities and a very weak finite growth of shear. Away from the zeros there is still a slow increase in shear but the velocities remain constant. Although away from zeros the shear does become infinite at the singularity, in the oceanic context the growth rate seems to be too slow, and so far neglected processes might arrest and reverse the growth. Evolution in the middle waveguide illustrated in figure 6 has three important distinctions. First, the WKB remains valid over the whole domain including the singularity. Second, the amplitude growth is stronger: the account of dispersion weakens it, but velocity continues to grow mildly for about 400 km. The small $\hat{y}$ asymptotics do not catch this growth. The last and the most important distinction is that the growth of vertical shear is stronger; shear tends to infinity at the tipping latitude, although the initial growth rate is quite moderate. Again it should be noted that this consideration is carried out at the zero of the eigenfunction for $n = 1$, while the growth rates are higher away from the zero. We evaluate the function at this point for simplicity, as any other constant value of z would leave the waveguide before reaching the singularity; to follow the line of maximal shear is complicated and could be confusing without elaborating it in great detail.

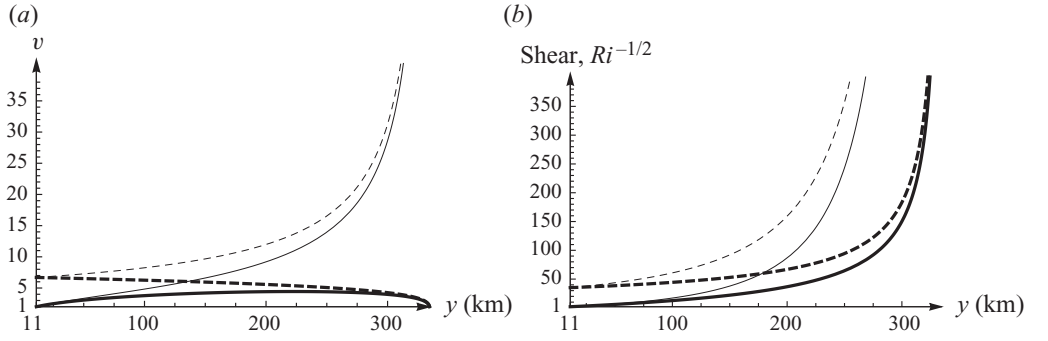

FIGURE 6. Middle waveguide: meridional velocity (a) and the vertical shear or $Ri^{-1/2}$ (b). Solid lines represent the full WKB results, dashed lines show their small $\hat{y}$ asymptotics. Evolution of monochromatic wave is plotted in thin lines. Finite bandwidth results are shown in thick lines. The curves are normalised by choosing a_0 such that the full WKB expressions (solid line) equal one at the chosen starting point y_{start}. Parameters used: $z = z_m$, $y_{start} = 11$ km, $\phi = 45°$, $N_0 = 3.3 \times 10^{-4}$ s^{-1}, $h = 100$ m.

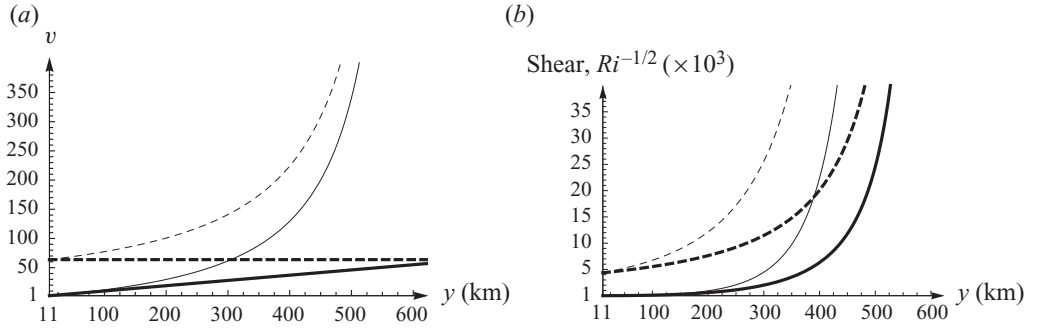

FIGURE 7. Bottom waveguide: meridional velocity (a) and the vertical shear or $Ri^{-1/2}$ (b). Solid lines represent the full WKB results, dashed lines show their small $\hat{y}$ asymptotics. Evolution of monochromatic wave is plotted in thin lines. Finite bandwidth results are shown in thick lines. The curves are normalised by choosing a_0 such that the full WKB expressions (solid line) equal one at the chosen starting point y_{start}. Parameters used: $z = 0$, $y_{start} = 11$ km, $\phi = 45°$, $N_0 = 2.5 \times 10^{-4}$ s^{-1}, $h = 650$ m.

The same features are much more strongly pronounced in the case of the bottom waveguide as shown in figure 7: velocity grows linearly up to the singularity, and again the asymptotics fails to describe this growth. The shear grows much more substantially and exhibits singularity at the attractor latitude. For the same simple reasoning, the shear is evaluated at the bottom ($z = 0$), which is a zero of the eigenfunction. The asymptotics accurately predict the evolution in the vicinity of the attractor latitude and so can be used for demonstrating qualitative behaviour. What happens in the vicinity of the attractor latitude requires a more detailed consideration which we carry out below.

4.4.2. *Asymptotics in the vicinity of the singularity*

Asymptotics in the vicinity of the attractor latitude in terms of the distance to the critical point $\hat{y}$ have the following universal form for all physical variables of interest:

$$\text{Variable of interest} \sim \hat{y}^{-m_j} \hat{\Phi}_j \, \mathrm{e}^{\mathrm{i}(c\hat{y}^{-k} - \sigma t + \delta z)}, \quad c = \text{const.} \tag{4.17}$$

Waveguide/variable	$\hat{\Phi}_1$	$\hat{\Phi}_2$	$\hat{z}$	A	l	c_g	k
Bottom$_{(mc)}$	$\mathrm{Ai}(\hat{z})$	$\partial_{\hat{z}}\mathrm{Ai}(\hat{z})$	$\hat{y}^{-1}z - s_n$	$\hat{y}^{-1/4}$	$\hat{y}^{-3/2}$	$\hat{y}^{5/2}$	3/2
Bottom$_{(fb)}$	$\mathrm{Ai}(\hat{z})$	$\partial_{\hat{z}}\mathrm{Ai}(\hat{z})$	$\hat{y}^{-1}z - s_n$	$\hat{y}^{1}$	$\hat{y}^{-3/2}$	$\hat{y}^{5/2}$	3/2
Middle$_{(mc)}$	$\mathrm{e}^{-\hat{z}^2/2}\mathscr{H}_n(\hat{z})$	$\mathrm{e}^{-\hat{z}^2/2}\partial_{\hat{z}}\mathscr{H}_n(\hat{z})$	$\hat{y}^{-1/2}z$	$\hat{y}^{-1/4}$	$\hat{y}^{-1}$	$\hat{y}^{2}$	1
Middle$_{(fb)}$	$\mathrm{e}^{-\hat{z}^2/2}\mathscr{H}_n(\hat{z})$	$\mathrm{e}^{-\hat{z}^2/2}\partial_{\hat{z}}\mathscr{H}_n(\hat{z})$	$\hat{y}^{-1/2}z$	$\hat{y}^{3/4}$	$\hat{y}^{-1}$	$\hat{y}^{2}$	1
Top$_{(mc)}$	$\sin(\hat{z})$	$\cos(\hat{z})$	z	$\hat{y}^{-1/4}$	$\hat{y}^{-1/2}$	$\hat{y}^{3/2}$	1/2
Top$_{(fb)}$	$\sin(\hat{z})$	$\cos(\hat{z})$	z	$\hat{y}^{1/2}$	$\hat{y}^{-1/2}$	$\hat{y}^{3/2}$	1/2

TABLE 1. Asymptotics for the basic quantities in each waveguide. The subscripts '*mc*' and '*fb*' indicate the monochromatic and finite bandwidth wavepackets, respectively. A is the normalised streamfunction amplitude.

Waveguide/variable	w	v	u	b	p	ε_N	v_z, u_z	Ri^{-1}
Bottom$_{(mc)}$	7/4	7/4	7/4	7/4	1/4	13/4	13/4	13/2
Bottom$_{(fb)}$	1/2	1/2	1/2	1/2	−1	2	2	4
Middle$_{(mc)}$	5/4	5/4	5/4	5/4	1/4	9/4	9/4	9/2
Middle$_{(fb)}$	5/4	1/4	1/4	1/4	−3/4	5/4	5/4	5/2
Top$_{(mc)}$	3/4	3/4	3/4	3/4	1/4	5/4	5/4	5/2
Top$_{(fb)}$	0	0	0	0	−1/2	1/2	1/2	1/2

TABLE 2. The exponents m_1 for generic small $\hat{y}$ asymptotics (4.17). Here p denotes the variation of pressure over reference density and ε_N is nonlinearity small parameter. The subscripts '*mc*' and '*fb*' indicate the monochromatic and finite bandwidth wavepackets, respectively.

Waveguide/variable	w	v	u	b	p	ε_N	v_z, u_z	Ri^{-1}
Bottom$_{(mc)}$	–	5/4	5/4	–	−1/4	11/4	11/4	11/2
Bottom$_{(fb)}$	–	0	0	–	−3/2	3/2	3/2	3
Middle$_{(mc)}$	–	3/4	3/4	–	−1/4	7/4	7/4	7/2
Middle$_{(fb)}$	–	−1/4	−1/4	–	−5/4	3/4	3/4	3/2
Top$_{(mc)}$	–	1/4	1/4	–	−1/4	3/4	3/4	3/2
Top$_{(fb)}$	–	−1/2	−1/2	–	−1	0	0	0

TABLE 3. The exponents m_2 for a small $\hat{y}$ asymptotic (4.17) near the boundary (for the top and bottom waveguide) and in the vicinity of the symmetry line for the middle waveguide. The subscripts '*mc*' and '*fb*' indicate the monochromatic and finite bandwidth wavepackets, respectively. The notation is the same as in table 2. Near the boundaries and zeros of the eigenfunctions the quantities w and b do not have an expansion in $\hat{y}$ and are approximately zero.

The expression for $\hat{\Phi}_j$, exponents m_j and k as well as constant c are different for each waveguide. The exponents m_j also differ for monochromatic and finite bandwidth packets. The subscript $j = 1$ indicates the generic asymptotic regime given by the leading-order asymptotic term which vanishes at the zeros of the eigenfunction. Their positions include the 'bottom' boundaries for the top and bottom waveguides for all modes and the symmetry line for the middle waveguide for the odd nodes; correspondingly the formulae with $j = 1$ describe the wave field away from these zeros. The subscript $j = 2$ indicates the near-zero asymptotic regime. Results are summarised in tables 1–3. The expressions for the coefficients can be found by taking the streamfunction coefficients given in Appendix A and using the streamfunction

definition (2.6) and the Euler equations (2.4*a*)–(2.4*e*). An example is given in Appendix B.2 for vertical shear in the bottom waveguide.

It is worth noting that the growth of all field components is the most robust for the bottom waveguide and weakest for the top waveguide. In all waveguides in the monochromatic case there is an infinite increase in velocities and shear towards singularity in both the generic and near-zero asymptotics. Taking into account the realistic effect of finite bandwidth does not destroy the phenomenon of the singular focusing, but vastly changes its outcome, as previously discussed. The finite bandwidth effects each waveguide differently. For the bottom waveguide, while growth of all field variables continues for most of the domain, the growth of velocities is slowed down near the zeros of the eigenfunction $\hat{\Phi}_1$, producing regions of near-zero growth in the y–z domain. However, the vertical shear and inverse Richardson number continue to grow robustly even according to the near-zero asymptotics. The velocities in the middle waveguide also continue to grow while away from the zeros; however, according to the near-zero asymptotics the velocities decay at the same rate as they increase under the generic asymptotics. Importantly, however, both the vertical shear and inverse Richardson number continue to grow, albeit more slowly than in the bottom waveguide. Finally, for the upper waveguide the velocities are nearly constant ($\sim\hat{y}^0$) in the generic case and are decreasing in the vicinity of zeros. The shear increases away from the zeros and is asymptotically constant in their neighbourhood. Although the inverse Richardson number is growing, the growth is much slower than in the other waveguides.

For all the waveguides of special interest is the effect of nearby zeros on the shear and inverse Richardson number. If we move the 'observation point' z off $z=z_m$ for the middle waveguides and $z=0$ for the bottom waveguide the local buoyancy frequency N will increase thus decreasing the inverse Richardson number. However, since the $z=z_m$ and $z=0$ for their respective waveguides coincide with a zero in the eigenfunction (for all modes on the top and bottom waveguides and for odd modes on the middle waveguide), the growth of inverse Richardson number at these points will be minimal (see tables 2 and 3). This implies that the maximum of inverse Richardson number which is initially at $z=z_m$ (or $z=0$) then moves onto the generic asymptotics, which provides local maximum in inverse Richardson number growth. For higher mode numbers, this creates alternating regions of high and low shear in the vertical cross-sections and causes non-monotonic growth in y of the inverse Richardson number for any fixed z.

5. Discussion

We begin by summarising our findings from the basic fluid dynamics perspective. For inertia-gravity waves in a rotating ideal fluid with arbitrary density stratification confined in a spherical shell we analytically found singular modes of continuous spectrum within the framework of the linearised Euler equations on the non-traditional β-plane. More specifically, first we noticed that the wavelength of inertia-gravity waves is rapidly decreasing polewards of the inertial latitude, which implies that beyond the inertial latitude there is always separation of scales between the wavelength and the curvature radius of the surface R, whatever the value of R. This separation of scales is exploited, allowing an analytic solution of the mixed-type boundary value problem to be obtained in the WKB description. For waves of a fixed frequency σ the solutions become singular at the tipping points of the hyperbolicity domain y^*. Depending on the stratification profile we identified three

generic basic types of waveguides and corresponding tip singularities: 'wedge-like', 'parabolic' and 'corner'; in the oceanic context they appear as the bottom, mid-ocean and top guides. For an arbitrary smooth stratification profile, the wave motion becomes confined in the waveguides and then focuses at their tips. The particular way the wave focuses is prescribed by the stratification in the vicinity of the tip. Locally, the buoyancy frequency $N(z)$ could be either constant, linear, quadratic or non-analytic. The explicit analytic solutions in the vicinity of these singularities summarised in § 4.4.2 are universal in the sense that they describe the generic options for an arbitrary smooth stratification. Qualitatively the wave evolution resembles the classical problem of an internal wave approaching its critical layer (e.g. LeBlond & Mysak 1978; Miropol'sky 2001): within the framework of the initial-value problem a wavepacket never reaches the singular point, while the wavelength tends to zero. However, in contrast to the critical layer situation, where reflection and penetration are possible for relatively weak stratification with $Ri \sim 1$ (e.g. Lindzen Barker 1985), in our case there is no reflection, even in the ideal fluid the singularities act as absolute absorbers of the wave field, similar to the black holes in astrophysics. There are also important distinctions of mathematical character: critical layers for internal waves are considered as one-dimensional problems described by ODEs, while our singularities are two-dimensional and have to be described by mixed-type PDEs. Although two-dimensional absorbing critical layers are also known in the context of Rossby waves on zonal currents (Gnevyshev & Shrira 1989), their mathematical model is essentially different.

The second key question is how robust are the found singularities. Since each Fourier harmonic develops a singularity at its own tipping latitude, survival of the singularities for a finite bandwidth wavepacket and, hence, their physical existence is not *a priori* guaranteed. We demonstrated that the singularities are robust in this sense, they are weakened but not smoothed out by the finite bandwidth of the packet. It could also be proved that the found singularities are not an artefact of the β-plane description and accurately capture the field behaviour in full spherical geometry. However, the proof requires a special consideration and therefore will be given elsewhere. The main general conclusion is that the evolution of inertia-gravity waves beyond the inertial latitude leads to irreversible shrinkage of scales and infinite growth of vertical shear. Whether this growth could cause mixing, or neglected nonlinearity and diffusion will interfere earlier, cannot be discussed in a general setting: the question has to be addressed only on a case-by-case basis with respect to a specific context. Below we discuss it for internal waves in the ocean.

For inertia-gravity waves in the ocean we have described a mechanism leading to the increase of vertical shear, which can be a potential cause of mixing. We have also got a good overall picture of wavepacket evolution in each of the three subinertial waveguides typical for the oceanic stratification. The key open question of how relevant these findings are to a real ocean cannot be adequately addressed within the scope of the present paper since the rate of increase of vertical shear has to be compared to the neglected processes (e.g. turbulent viscosity, bottom friction, nonlinear interactions), which requires a special consideration and will be reported elsewhere. However, if the shear increases sufficiently fast this mechanism will likely be unaffected by other factors. Thus finding the rate of shear growth and analysing its dependence on the environmental parameters might provide us with an insight into the potential importance of this mechanism for the real ocean even without consideration of other factors. The task of mapping the parameter space is not trivial. Even for the simplified models of stratification the buoyancy

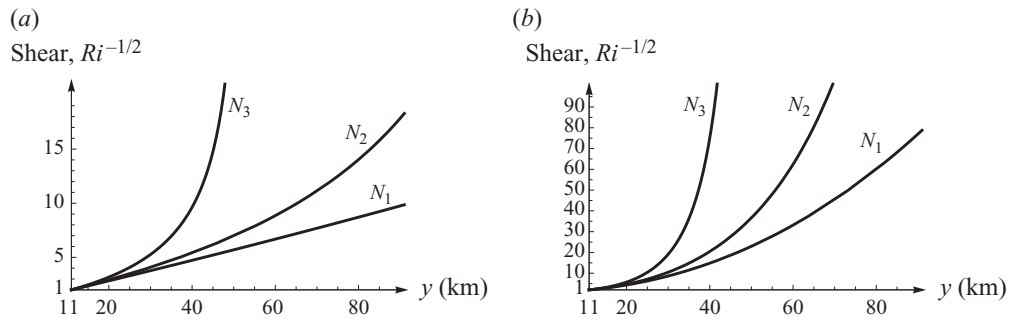

FIGURE 8. Normalised vertical shear or $Ri^{-1/2}$ for the middle (a) and bottom (b) waveguides. The increase in buoyancy frequency reduces the maximum length of the waveguide (see figure 3). The sample values of N_0: $N_1 = 2 \times 10^{-4}\,\mathrm{s}^{-1}$, $N_2 = 4 \times 10^{-4}\,\mathrm{s}^{-1}$ and $N_3 = 6 \times 10^{-4}\,\mathrm{s}^{-1}$. Parameters used: $z = 0$, $y_{start} = 11\,\mathrm{km}$, $\phi = 45^\circ$, $h = 650\,\mathrm{m}$ (bottom waveguide) and $h = 104\,\mathrm{m}$ (middle waveguide). The inertial latitude is at $y = 0$.

frequency $N(z)$ employed in the vicinity of the singularity, $N(z)$ is characterised by two parameters: its minimal value N_0 and vertical scale of inhomogeneity h. We recall that we estimate h from the profile assuming linear dependence on z near the bottom ($\gamma_1 = N_0^2/h$), quadratic dependence at the centre of the middle guide ($\gamma_2 = N_0^2/h^2$) and for the top guide we set h equal to the thickness of the guide. The latitude ϕ specifies two other frequency scales: f and $\tilde{f}$. If we non-dimensionalise our results by setting, say, $f = 1$, the gain in simplicity is immaterial, we still have to deal with multi-dimensional parameter space, but it becomes less convenient to interpret the results of the analysis in terms of dimensional quantities commonly used for describing the observations. We find the use of standard dimensional variables to be more illuminating.

The growth of vertical shear for the bottom and middle waveguides depends most upon buoyancy frequency N_0. The dependence is illustrated in figure 8 for several values of N_0. To interpret better the parameter space we introduce a length scale characterising the increase in the vertical shear denoted L_{foc}. For the bottom and middle waveguides, where there is a significant increase in shear, the length L_{foc} is defined as the distance required for the shear to double from its initial value. For the top waveguide, where the shear does not increase dramatically, we define L_{foc} as the inverse rate of change of vertical shear with y normalised at the starting point y_{start}. For all waveguides this is done at the maximum of vertical shear in the initial vertical cross-section. This maximum occurs at specific depths: $z = z_m$ for the middle waveguide and at the lower boundary $z = 0$ for the top and bottom waveguides. At these particular depths the vertical shear $|\boldsymbol{u}_z| = \sqrt{|u_z|^2 + |v_z|^2}$ has an explicit dependence upon the parameter h in the form

$$|\boldsymbol{u}_z(N_0, \phi, y, z, t, h)| = P(h)Q(N_0, \phi, y)\exp \mathrm{i}(ly - \sigma t + \delta z), \tag{5.1}$$

where the functions P and Q are different for each waveguide (see Appendix B.1 for details). Therefore the dependence on h drops out for the length scale L_{foc}. We are not interested in the 'wave' part of the solution and so we take the absolute value of the shear. In figure 9 the length scale L_{foc} is shown for the middle and the bottom waveguides for a wide range of parameters.

Evolution in the top waveguide has a very weak dependence upon stratification and L_{foc} is of the order of $10^6\,\mathrm{m}$ initially. The shear does increase albeit very slowly,

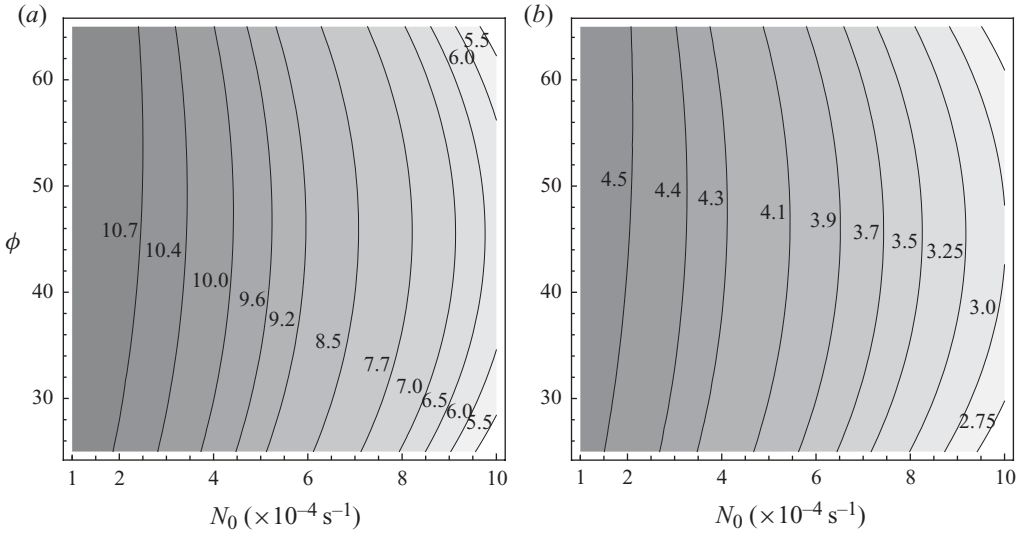

FIGURE 9. Dependence of L_{foc} (in kilometres) on N_0 (s^{-1}) and latitude ϕ (degrees) for the middle (a) and bottom (b) waveguides. The parameters are the same as in figure 8, and taken at the initial starting point $y_{start} = 11$ km.

and most likely the increase is too small to be of significance for the mixed-layer dynamics. At the same time, a single-layer model with constant N being a basic model for rotating stratified fluids certainly could be applicable to a wide range of situations well beyond the context of the oceanic mixed layer.

Although the length scale L_{foc} is a useful characteristics of spatial shear growth rate, a temporal growth rate would be more informative, since it would allow direct comparisons with the time scales of other processes not considered in our study. It is straightforward to convert the results from spatial to temporal frame via (4.4). The dependence of the shear growth rate inverse time scale T_{foc}, which we define as the number of wave periods required for the wavepacket to double its vertical shear, is presented in figure 10 for the middle and bottom waveguides. In contrast to the spatial growth rate in figures 8 and 9, the temporal growth rate increases with the decrease of N_0. For a fixed N_0 it decreases with latitude. It is easy to see that for the bottom waveguide there is a wide range of parameters where the shear growth rate is so high that it is unlikely that any other mechanisms might arrest or reverse the growth, preventing expected wave breaking. The shear growth in the middle waveguide is much slower, and hence the possibility of wave breaking caused primarily by this mechanism is reduced. It should be noted that in both these waveguides the maximum of vertical shear is initially located at the same depth z as the corresponding attractor, which coincides with a zero of the eigenfunction. Although the near-zero asymptotics are slower than the generic asymptotics, the initial growth appears to be greatest at these points. This is because far from the tipping latitude the asymptotics are not valid yet, just as the initial growth of meridional velocity is not captured by the asymptotics (see figure 6).

To discuss the potential impact of this mechanism we would have to consider simultaneously other physical mechanisms relevant to the time scales in question, which goes beyond the scope of the present work. Note that in contrast to the spatial scale L_{foc}, the time scale T_{foc} depends upon the scale of vertical inhomogeneity h, since

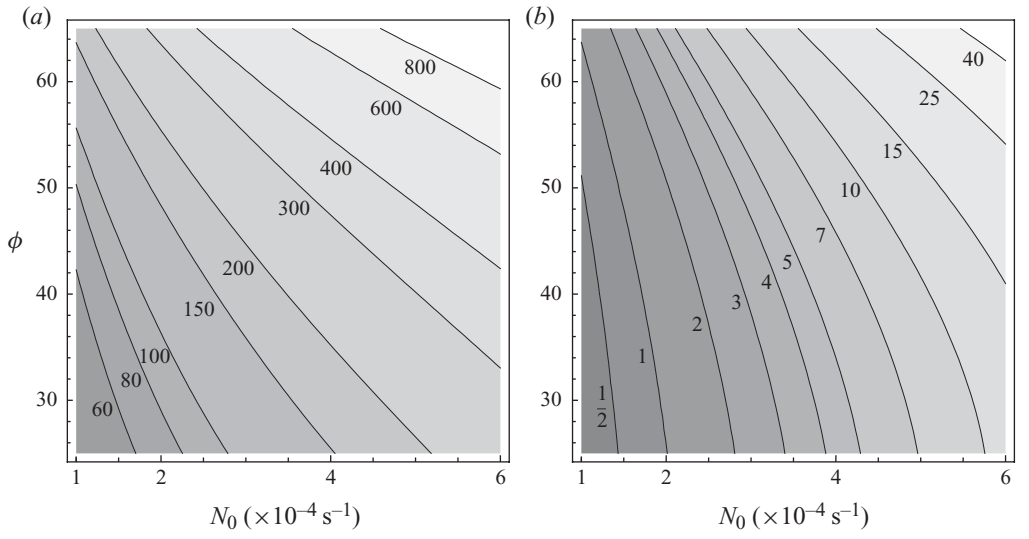

FIGURE 10. Number of periods T_{foc} needed for the vertical shear to double and Ri^{-1} to quadruple for the middle (a) and bottom (b) waveguides. The parameters and units are the same as in figure 8, and taken at the initial starting point y_{start}.

the transformation into the temporal frame involves h-dependent group velocity. The dependence on h is very simple, since the group velocity is proportional to h; h simply represents a rescaling of time. In particular, note that the minima of T_{foc} in (N_0, ϕ) space will remain minima for any h. Away from the depths chosen for the figures the dependence upon h is much more complicated. Since h is the characteristic vertical scale of inhomogeneity it determines the initial width of the waveguide and hence the portion of energy this guide will capture. Since the distance to singularity does not depend on h, an increase in h implies faster spatial contraction of the wave vertical scale.

Summarising our findings, we can conclude that for a wide range of parameters typical of the real ocean the mechanism we considered is expected to provide robust growth of vertical shear in the bottom waveguide, much weaker growth in the middle waveguide and even weaker growth in the top waveguide. At present, we do not have experimental evidence to support our conclusions although the already existing experimental techniques like the acoustic Doppler current profiler (ADCP) in principle allow direct verification (e.g. Van Haren 2006). To outline more accurately the range of parameters, where intense mixing is the most likely outcome of wave evolution, one has to take into account other physical mechanisms, which are the subject of further studies.

At the same time it has to be mentioned that all the above estimates were made for an ocean with no background flows. The key element of the vertical shear growth we investigated is horizontal inhomogeneity, which has so far been provided by the gradient of the planetary vorticity β. The presence of large-scale background circulation could cause a much stronger inhomogeneity, significantly changing the overall picture of wave evolution and the corresponding estimates. To get quantitative estimates, it is necessary to solve a much more involved problem of wave propagation on a sheared current, which goes beyond the scope of this paper.

Appendix A. Inviscid asymptotics in the vicinity of the singularity (small $\hat{y}$) and inertial latitude (small y)

Here we express the amplitude constants for both the small $\hat{y}$ asymptotics (3.31), (3.37) and (3.39) and the small y asymptotics in terms of initial amplitude a_0. For brevity we will use the following parameters and notations: $y^\star$ is the distance from the inertial latitude to the singular point specified by (3.9); y_{start} is the 'starting point', the distance past the inertial latitude at the boundary of the WKB validity which we choose as the initial location of the wavepacket under consideration; $\hat{\Delta}$ and $\hat{f}$ denote combinations of parameters given by the expressions

$$\hat{\Delta} = 2(f_0 + \beta y_{start})\beta\left(N_0^2 - \sigma_0^2\right), \tag{A 1}$$

$$\hat{f}^{\,2} = (f_0 + \beta y_{start})^2 + 2(f_0 + \beta y_{start})\beta y^\star + \beta^2 (y^\star)^2. \tag{A 2}$$

A.1. *Bottom waveguide*

For the small $\hat{y}$ asymptotics, we have

$$\alpha_{\hat{y}} = a_0 \left[\hat{l}^{1/3} \left(\frac{\hat{f}^2 - \sigma_0^2}{\gamma_1} \right)^{1/3} \hat{\Delta} \frac{A_n}{\sigma^2 - \bar{f}^2} + \gamma_1 \left(\frac{\hat{f}^2 - \sigma_0^2}{\gamma_1} \right)^{2/3} \hat{l}^{-1/3} (B_n)^{2/3} \right]^{-1/2}, \tag{A 3}$$

where

$$A_n = \int_0^\infty \mathrm{Ai}[z - s_n]^2 \, \mathrm{d}z, \quad A_1 = 0.4917,\ A_2 = 0.6450,\ A_3 = 0.7486, \tag{A 4}$$

$$B_n = \int_0^\infty z\mathrm{Ai}[z - s_n]^2 \, \mathrm{d}z, \quad B_1 = 0.7664,\ B_2 = 1.7578,\ B_3 = 2.7550. \tag{A 5}$$

The expression for α_l is related to $\alpha_{\hat{y}}$ via the simple formula

$$\alpha_l = \alpha_{\hat{y}} \hat{l}^{-1/6}, \quad \text{where} \quad \hat{l} = \gamma_1 (\hat{f}^2 - \sigma^2)^2 \left(\frac{s_n}{\hat{\Delta}} \right)^{3/2}. \tag{A 6}$$

For the small y asymptotics we have

$$a_{(\Phi)} \sim \alpha_y (y + y_{start})^0 = a_0 \left[-\bar{l}^{1/3} \left(\frac{2 f_0 \beta}{\gamma_1} \right)^{1/3} \sigma^2 \tilde{f}^2 \frac{A_n}{2 f_0 \beta} + \gamma_1 \left(\frac{2 f_0 \beta}{\gamma_1} \right)^{2/3} \bar{l}^{-1/3} B_n \right]^{-1/2} (y + y_{start})^0, \tag{A 7}$$

$$\bar{l} = 4\gamma_1 f_0^2 \beta^2 \left(\frac{s_n}{\sigma^2 \tilde{f}^2} \right)^{3/2}. \tag{A 8}$$

A.2. *Middle waveguide*

For the small $\hat{y}$ asymptotics, we have

$$\alpha_{\hat{y}} = a_0 \left[\frac{-\hat{l}\hat{\Delta}}{\sigma_0^2 - \hat{f}^2} \left(\frac{\hat{f}^2 - \sigma_0^2}{\hat{l}^2 \gamma_2} \right)^{1/4} A_n - \gamma_2 \hat{l} \left(\frac{\hat{f}^2 - \sigma_0^2}{\hat{l}^2 \gamma_2} \right)^{3/4} B_n \right]^{-1/2}, \tag{A 9}$$

where

$$A_n = \int_{-\infty}^{\infty} \exp(-\hat{z}^2) H_n(\hat{z})^2 \, \mathrm{d}\hat{z}, \quad A_1 = 2\sqrt{\pi}, \ A_2 = 8\sqrt{\pi}, A_3 = 48\sqrt{\pi}, \tag{A 10}$$

$$B_n = \int_{-\infty}^{\infty} \hat{z}^2 \exp(-\hat{z}^2) H_n(\hat{z})^2 \, \mathrm{d}\hat{z}, \quad B_1 = 3\sqrt{\pi}, \ B_2 = 20\sqrt{\pi}, B_3 = 168\sqrt{\pi}. \tag{A 11}$$

The expression for α_l is related to $\alpha_{\hat{y}}$ via the simple formula

$$\alpha_l = \alpha_{\hat{y}} \hat{l}^{-1/4}, \quad \text{where} \quad \hat{l} = \frac{1}{\hat{\Delta}}(2n+1)\sqrt{\gamma_2}\left(\hat{f}^2 - \sigma_0^2\right)^{3/2}. \tag{A 12}$$

The small y asymptotics are

$$a_{(\Phi)} \sim \alpha_y (y + y^\star)^0 y = a_0 \left[\frac{\sigma^2 \tilde{f}^2 \bar{l}}{-2 f_0 \beta} \left(\frac{2 f_0 \beta}{\gamma_2 \bar{l}^2} \right)^{1/4} A_n + \gamma_2 \bar{l} \left(\frac{2 f_0 \beta}{\gamma_2 \bar{l}} \right)^{3/4} B_n \right]^{-1/2} (y + y_{start})^0, \tag{A 13}$$

$$\bar{l} = -(2n+1)\gamma_2^{1/2} \frac{(2 f_0 \beta)^{3/2}}{\sigma^2 \tilde{f}^2}. \tag{A 14}$$

A.3. *Upper waveguide*

For the small $\hat{y}$ asymptotics we have

$$\alpha_{\hat{y}} = a_0 \left(\frac{\hat{l}\hat{\Delta}}{\hat{f}^2 - \sigma_0^2} A_n \right)^{-1/2}, \tag{A 15}$$

where

$$A_n = \int_0^H \sin\left(\frac{n\pi z}{H} \right)^2 \mathrm{d}z = \frac{H}{2} \ \forall n. \tag{A 16}$$

The expression for α_l is related to $\alpha_{\hat{y}}$ as

$$\alpha_l = \alpha_{\hat{y}} (\hat{l})^{-1/2}, \quad \text{where} \quad \hat{l} = \frac{1}{\hat{\Delta}} \frac{n\pi}{H} \left(\sigma_0^2 - \hat{f} \right). \tag{A 17}$$

The small y asymptotics yield

$$a_{(\Phi)} \sim \alpha_y (y + y_{start})^0 = a_0 \left(\frac{\bar{l} \sigma^2 \tilde{f}^2}{2 f_0 \beta} A_n \right)^{-1/2} (y + y_{start})^0, \quad \bar{l} = \frac{2n\pi f_0 \beta}{H \sigma \tilde{f}}. \tag{A 18}$$

Appendix B. Derivation of vertical shear for bottom waveguide

Here we show an example of the derivation of the asymptotics for total vertical shear in the bottom waveguide. The total vertical shear is composed of both the derivative of zonal and meridional velocity. From the definition of the streamfunction (2.6) and its modal solution (3.10) the vertical shear of meridional velocity is

$$v_z = \psi_{zz} = a_\Phi (-\delta^2 \Phi + 2\mathrm{i}\delta \tilde{l}^{2/3} \Phi' + \tilde{l}^{2/3} (\tilde{l}^{2/3} z - s_n) \Phi) E, \tag{B 1}$$

where a_Φ is the amplitude and

$$\Phi = \mathrm{Ai}\left[\tilde{l}^{2/3} z - s_n \right], \quad \Phi' = \mathrm{Ai}'\left[\tilde{l}^{2/3} z - s_n \right], \quad E = \exp \mathrm{i}(ly - \sigma t + \delta z). \tag{B 2}$$

From the first Euler equation (2.4*a*) and by assuming the usual harmonic dependence on time with frequency σ, the vertical shear of zonal velocity is given by

$$u_z = \frac{\partial}{\partial z}\left[\frac{a_\Phi}{\mathrm{i}\sigma}(fv - \tilde{f}w)\right] \tag{B 3}$$

$$= \frac{a_\Phi}{\mathrm{i}\sigma}\left[\Phi\left(f\tilde{l}^{2/3}\left(\tilde{l}^{2/3}z - s_n\right) - \delta(f\delta + \tilde{f}l)\right) + \mathrm{i}\Phi'\tilde{l}^{2/3}(2f\delta + \tilde{f}l)\right]E. \tag{B 4}$$

The total vertical shear is then $|\boldsymbol{u}_z| = \sqrt{|u_z|^2 + |v_z|^2}$.

B.1. *Dependence upon height h*

The dependence of the vertical shear upon h is quite simple at the bottom boundary $z = 0$. At this point the eigenfunction and its derivative become

$$\Phi = \mathrm{Ai}\left[\tilde{l}^{2/3}z - s_n\right] = \mathrm{Ai}[-s_n] = 0, \quad \Phi' = \mathrm{Ai}'\left[\tilde{l}^{2/3}z - s_n\right] = \mathrm{Ai}'[-s_n] \neq 0. \tag{B 5}$$

This reduces the meridional and zonal velocity derivatives to

$$v_z = a_\Phi\left(2\mathrm{i}\delta\tilde{l}^{2/3}\Phi'\right)E, \quad u_z = a_\Phi\frac{1}{\sigma}\left[\tilde{l}^{2/3}(2f\delta + \tilde{f}l)\Phi'\right]E, \tag{B 6}$$

giving a total vertical shear of

$$|\boldsymbol{u}_z| = \sqrt{|u_z|^2 + |v_z|^2} = \frac{a_\Phi}{\sigma}(4\delta^2(f^2 + \sigma^2) + \tilde{f}^2l^2 + 4f\tilde{f}\delta l)^{1/2}\tilde{l}^{2/3}\Phi'E$$

$$= \frac{a_\Phi\tilde{f}N_0^4}{h^2\sigma}\sqrt{f^4 + \sigma^4 + 6f^2\sigma^2}(f^2 - \sigma^2)^2\left(\frac{s_n}{\Delta}\right)^{5/2}\Phi'E. \tag{B 7}$$

Here we are concerned only with the amplitude of the vertical shear, and so we take the absolute value. It should be noted that a_Φ does not depend upon h in any of the waveguides. This can be seen by substituting the expressions for l, δ, $\tilde{l}$ and b into the formulae for a_Φ. From here it is clear that the dependence upon h is simple, and that by normalising the shear we effectively remove the dependence. The same is true of the top and middle waveguides, with the same h^{-2}-dependence.

B.2. *Asymptotics*

In this section, we will be using the expressions for the asymptotic constants given in Appendix A. To find the asymptotics for vertical shear in the bottom waveguides we first start by introducing the parameter $\hat{y} = y^\star - y$ as the distance to the singularity. Now at $z = 0$ and $\hat{y} = 0$, we are at the attractor latitude which for this guide coincides with the tipping latitude, and so the hyperbolicity condition is satisfied. Using this we find that the leading asymptotics for the wavenumber is

$$l \sim \hat{l}\hat{y}^{-3/2}, \quad \hat{l} = \gamma_1(\hat{f}^2 - \sigma^2)^2\left(\frac{s_n}{\hat{\Delta}}\right)^{3/2}. \tag{B 8}$$

Putting this along with the expressions for δ and $\tilde{l}$ into the derivatives of velocity (B 1), (B 4) along with the expression for the amplitude (A 3) gives us

$$v_z \sim \alpha_{\hat{y}}\left\{\Phi\left[\frac{\gamma_1^{1/3}\hat{l}^{2/3}}{(\hat{f}^2 - \sigma^2)^{1/3}}\left(\frac{\gamma_1^{1/3}\hat{l}^{2/3}}{(\hat{f}^2 - \sigma^2)^{1/3}}z\hat{y}^{-9/4} - s_n\hat{y}^{-5/4}\right)\right.\right.$$

$$\left.\left. - \frac{\hat{f}^2\tilde{f}^2\hat{l}^2}{(\hat{f}^2 - \sigma^2)^2}\hat{y}^{-13/4}\right] - \Phi'\frac{2\mathrm{i}\hat{f}\tilde{f}\hat{l}^{5/3}\gamma_1^{1/3}}{(\hat{f}^2 - \sigma^2)^{4/3}}\hat{y}^{-11/4}\right\}E, \tag{B 9}$$

$$u_z \sim \frac{\alpha_{\hat{y}}}{\mathrm{i}\sigma}\left\{\Phi\left[\frac{\hat{f}\gamma_1^{1/3}\hat{l}^{2/3}}{(\hat{f}^2-\sigma^2)^{1/3}}\left(\frac{\gamma_1^{1/3}\hat{l}^{2/3}}{(\hat{f}^2-\sigma^2)^{1/3}}z\hat{y}^{-9/4}-s_n\hat{y}^{-5/4}\right)\right.\right.$$
$$\left.\left.+\frac{\hat{f}\tilde{f}\hat{l}}{\hat{f}^2-\sigma^2}\left(\tilde{f}\hat{l}-\frac{\hat{f}^2\tilde{f}\hat{l}}{\hat{f}^2-\sigma^2}\right)\hat{y}^{-13/4}\right]+\Phi'\frac{\mathrm{i}\gamma_1^{1/3}\hat{l}^{2/3}}{(\hat{f}^2-\sigma^2)^{1/3}}\left(\tilde{f}\hat{l}-\frac{2\hat{f}^2\tilde{f}\hat{l}}{\hat{f}^2-\sigma^2}\right)\hat{y}^{-11/4}\right\}E. \tag{B 10}$$

As can be seen in both derivatives of velocity, the leading-order asymptotic involves Φ while the second order involves Φ'. As such there are two asymptotical regimes: the generic regime where the leading-order term is $\hat{y}^{-13/4}$; and the slower $\hat{y}^{-11/4}$ regime when the eigenfunction Φ is zero. We will consider the total vertical shear $|\boldsymbol{u}_z| = \sqrt{|u_z|^2 + |v_z|^2}$ in these two regimes.

In the generic regime, we ignore all of the terms except the leading-order $\hat{y}^{-13/4}$ terms, giving

$$|\boldsymbol{u}_z| \sim \alpha_{\hat{y}}\frac{\hat{f}\tilde{f}^2\hat{l}^2}{\hat{f}^2-\sigma^2}\left(\frac{\hat{f}^2}{\hat{f}^2-\sigma^2}+\frac{1}{\sigma^2}\left(1-\frac{\hat{f}^2}{\hat{f}^2-\sigma^2}\right)^2\right)^{1/2}\hat{y}^{-13/4}E. \tag{B 11}$$

In the vicinity of a zero of the eigenfunction the leading-order terms disappear and the $\hat{y}^{-11/4}$ terms become leading-order, giving

$$|\boldsymbol{u}_z| \sim \alpha_{\hat{y}}\frac{\gamma_1^{1/3}\tilde{f}\hat{l}^{5/3}}{(\hat{f}^2-\sigma^2)^{1/3}}\left(\frac{4\hat{f}^2}{(\hat{f}^2-\sigma^2)^2}+\frac{1}{\sigma^2}\left(1-\frac{2\hat{f}^2}{\hat{f}^2-\sigma^2}\right)^2\right)^{1/2}\hat{y}^{-11/4}E. \tag{B 12}$$

The method is similar for the other waveguides. The asymptotic dependence of these field variables and all others with $\hat{y}$ can be found in tables 1–3.

REFERENCES

Abramowitz, M. & Stegun, I. A. 1965 *Handbook of Mathematical Functions*. Dover.

Alford, M. H. 2003 Redistribution of energy available for ocean mixing by long-range propagation of internal waves. *Nature* **423**, 159–162.

Danioux, E. & Klein, P. 2008 Propagation of wind energy into the deep ocean through a fully turbulent mesoscale eddy field. *J. Phys. Oceanogr.* **38**, 2224–2241.

Dintrans, B., Rieutord, M. & Valdettaro, L. 1999 Gravito-inertial waves in a rotating stratified sphere or spherical shell. *J. Fluid Mech.* **398**, 271–297.

Duffy, D. G. 2008 *Mixed Boundary Value Problems*. Chapman & Hall.

Fedoryuk, M. V. 1993 *Asymptotic Analysis*. Springer.

Friedlander, S. 1982 Turning surface behaviour for internal waves subject to general gravitational fields. *Geophys. Astrophys. Fluid Dyn.* **21**, 189–200.

Friedlander, S. & Siegmann, W. L. 1982 Internal waves in a rotating stratified fluid in an arbitrary gravitational field. *Geophys. Astrophys. Fluid Dyn.* **19**, 267–291.

Fu, L. L. 1981 Observations and models of inertial waves in the deep ocean. *Rev. Geophys. Space Phys.* **19** (1), 141–170.

Garrett, C. 2001 What is the 'near-inertial' band and why is it different from the rest of the internal wave spectrum? *J. Phys. Oceanogr.* **31** (4), 962–971.

Garrett, C. & St Laurent, L. 2002 Aspects of deep ocean mixing. *J. Oceanogr.* **58**, 11–24.

Gerkema, T. & Shrira, V. I. 2005*a* Near-inertial waves in the ocean: beyond the 'traditional approximation'. *J. Fluid Mech.* **529**, 195–219.

Gerkema, T. & Shrira, V. I. 2005*b* Near-inertial waves on the 'non-traditional' β-plane. *J. Geophys. Res. Oceans (JGR-C)* **110**, C01003.

Gerkema, T., Zimmerman, J. T. F., Mass, L. R. M. & van Haren, H. 2008 Geophysical and astrophysical fluid dynamics beyond the traditional approximation. *Rev. Geophys.* **46**. RG2004, doi:10.1029/2006RG000220.

Gnevyshev, V. G. & Shrira, V. I. 1989 Dynamics of Rossby-wave packets in the vicinity of zonal critical layer with the account of viscosity. *Izv. Acad. Sci. USSR Atmos. Ocean. Phys.* **25** (10), 1064–1074.

Greenspan, H. P. 1968 *The Theory of Rotating Fluids*. Cambridge University Press.

Grimshaw, R. H. J. 1975 A note on the β-plane approximation. *Tellus* XXVII, **4** 351–356.

Kasahara, A. 2009 A mechanism of deep-ocean mixing due to near-inertial waves generated by flow over bottom topography. *Dyn. Atmos. Oceans* **49**, 124–140.

Kumar, P. & Quataert, E. J. 1997 Angular momentum transport by gravity waves and its effect on the rotation of the solar interior. *ApJ* **475**, L143.

Kunze, E. 1985 Near-inertial wave-propagation in geostrophic shear. *J. Phys. Oceanogr.* **15** (5), 544–565.

LeBlond, P. H. & Mysak, L. A. 1978 *Waves in the Ocean*. Elsevier.

Leaman, K. D. 1976 Observation on vertical polarization and energy flux of near-inertial waves. *J. Phys. Oceanogr.* **6** (6), 894–908.

Lindzen, R. S. & Barker, J. W. 1985 Instability and wave over-reflection in stably stratified shear flow. *J. Fluid Mech.* **151**, 189–217.

Maas, L. R. M. & Harlander, U. 2006 Characteristics and energy rays of equatorially trapped, zonally symmetric internal waves. *Meteorol. Z.* **15** (4), 439–450.

Maas, L. R. M. 2001 Wave focusing and ensuing mean flow due to symmetry breaking in rotating fluids. *J. Fluid Mech*, **437**, 13–28.

Miropol'sky, Yu. Z. 2001 *Dynamics of Internal Gravity Waves in the Ocean*. Kluwer.

Munk, W. 1980 Internal wave spectra at the buoyant and inertial frequencies. *J. Phys. Oceanogr.* **10**, 1718–1728.

Pollard, R. T. & Millard, R. C. 1970 Comparison between observed and simulated wind-generated inertial oscillations. *Deep Sea Res.* **17**, 813–821.

Rieutord, M., Georgeot, B. & Valdettaro, L. 2001 Inertial waves in a rotating spherical shell: attractors and asymptotic spectrum. *J. Fluid Mech.* **435**, 103–144.

Staquet, C. 2004 Gravity and inertia-gravity internal waves: breaking processes and induced mixing. *Surv. Geophys.* **25**, 1573–0956.

Tricomi, F. G. 1954 *Lezioni sulle Equazioni a Derivate Parziali*. Editrice Gheroni Torino.

Van Haren, H. 2006 Asymmetrical vertical internal wave propagation. *Geophys. Res. Lett.* **33**, L06618.

Winters, K. B. & D'Asaro, E. A. 1997 Direct simulation of internal wave energy transfer. *J. Phys. Oceanogr.* **27**, 1937–1945.

Whitham, G. B. 1974 *Linear and Nonlinear Waves*. Wiley.

Wunsch, C. & Munk, W. 1998 Abyssal recipes. Part II. Energetics of tidal and wind mixing. *Deep-Sea Res.* **45** (12), 1977–2010.

Zahn, J.-P. 1997 Stellar rotation and mixing. In *Sounding Solar and Stellar Interiors: Proceedings of the 181st Symposium of the International Astronomical Union, Nice, France* (ed. J. Provost & F.-X. Schmider), 175–188, Kluwer.